ADVANCED MATERIALS
www.advmat.de

Lest We Forget–The Importance of Heteroatom Interactions in Heterocyclic Conjugated Systems, from Synthetic Metals to Organic Semiconductors

*Joseph Cameron, Alexander L. Kanibolotsky, and Peter J. Skabara**

The field of synthetic metals is, and remains, highly influential for the development of organic semiconductor materials. Yet, with the passing of time and the rapid development of conjugated materials in recent years, the link between synthetic metals and organic semiconductors is at risk of being forgotten. This review reflects on one of the key concepts developed in synthetic metals – heteroatom interactions. The application of this strategy in recent organic semiconductor materials, small molecules and polymers, is highlighted, with analysis of X-ray crystal structures and comparisons with model systems used to determine the influence of these non-covalent short contacts. The case is made that the wide range of effective heteroatom interactions and the high performance that has been achieved in devices from organic solar cells to transistors is testament to the seeds sown by the synthetic metals research community.

1. Introduction

The 1960s saw the onset of intense research into organic charge transfer salts and complexes as materials with intriguing conducting properties.[1] Many semiconductors were reported, but the overwhelming fascination was drawn by the realization of purely organic materials with metallic and even superconducting properties. There was a drive toward designing and preparing charge transfer materials with high temperature superconductivity and the prospect of processing synthetic wires. Thus, the concept of the "synthetic metal" was born and the field remains highly active today, despite enjoying its peak of activity from the 1970s to the 1990s. At that point in time, conjugated polymers were becoming recognized as a second type of organic conductor, initially with interest in their highly conductive properties and then as solution processable semiconductors that could be used in a wide range of device applications.[2] At the present time, organic semiconductor research dominates the field of "synthetic metals", at least in terms of the number of research groups and papers published in the area.

The International Conference on the Science and Technology of Synthetic Metals (ICSM) is a long-standing, biennial meeting which is arguably the largest of its type in the field.[3] At the recent 25th ICSM meeting in Glasgow (July 2022), the ICSM International Advisory Board held a meeting to discuss the future name of the conference series, since it was suggested that the current generation of researchers could not make a clear connection between the terms "synthetic metal" and "organic semiconductor", and therefore the title of the meeting could be made more appealing to early career researchers. Whilst a name-change will take place, it would be a deep pity if the origins of "synthetic metals" were forgotten, because the field still exists, and also because the community has built strongly on the discoveries made during the "synthetic metals" era. Perhaps not so obvious to all, some of the design strategies and understanding of bulk properties and self-assembly in "synthetic metals" have been carried over to conjugated molecules and polymers. This is perhaps overlooked by some researchers and means that further innovations into molecular design and insights into structure-property relationships of new materials may not benefit from key lessons already learned, leading to a "reinvention of the wheel". One of the most important characteristics of organic conductors is that their bulk properties are derived from heteroatom interactions between molecules and this phenomenon remains important in the design and properties of organic semiconductors. This review focuses on the nature and importance of these interactions in "synthetic metals" and semiconductors, and how we can apply strategies to control the conformation of molecules and their self-assembly in the solid-state toward enhanced bulk properties. Recognizing that the establishment and manipulation of such interactions is key to both types of materials is the purpose of this review, lest we forget the origin and the importance of the "synthetic metal".

J. Cameron, A. L. Kanibolotsky, P. J. Skabara
WestCHEM, School of Chemistry
University of Glasgow
University Avenue
Glasgow G12 8QQ, United Kingdom
E-mail: peter.skabara@glasgow.ac.uk
A. L. Kanibolotsky
Institute of Physical-Organic Chemistry and Coal Chemistry
Kyiv 02160, Ukraine

The ORCID identification number(s) for the author(s) of this article can be found under https://doi.org/10.1002/adma.202302259

DOI: 10.1002/adma.202302259

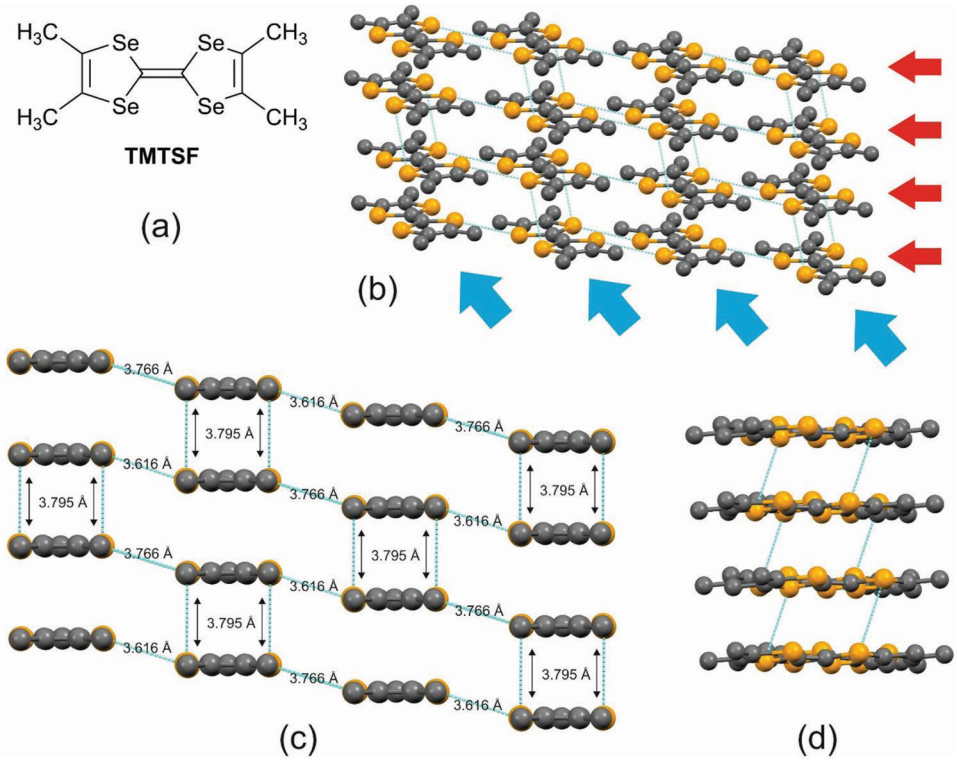

Figure 1. Structure and packing of TMTSF in the CT salt $(TMTSF)_2NO_3$: a) chemical structure; b) packing of TMTSF molecules showing Se···Se contacts; c) view showing the distances and 2D arrangement of short contacts between Se atoms (see the viewing directions of the blue arrows in 1b); d) view of a stack of TMTSF molecules, in which there are no Se···Se short contacts to the left or the right of the stack (see the viewing directions of the red arrows in 1b).

2. Heteroatom Interactions in Organic Charge Transfer Materials

Long-range interactions between molecules in a bulk organic solid are essential for efficient transport of holes and electrons. In this sub-section, we address two important features that influence bulk charge transport–namely, the nature and dimensionality of overlapping orbitals between molecules– and refer to organic charge transfer (CT) salts to emphasize these key points because they provide clear and unambiguous models. Dimensionality in organic materials is defined by the network of overlapping orbitals between molecules in the bulk, such that a 3D material has intermolecular orbital overlaps extending in all three cartesian directions. These "short contacts" between molecules are manifested through π-π or heteroatom interactions. Although the magnitude of electronic coupling is generally highest for 1D materials, charge transport is most efficient in 2D and 3D architectures.[2] In the quest for high conductivities and mobilities, a higher degree of dimensionality is desired, but 3D organic materials are extremely rare.[4] But what drives an organic conjugated material toward higher levels of dimensionality? Considering that long-range π-π short contacts are normally associated with planar molecules, simple flat molecules are limited to 1D stacked structures or 2D contacts through herringbone or rod-like packing.[2] In these cases, heteroatom interactions between molecules can provide an additional level of dimensionality or can even replace π-π as the mode for orbital overlap, but how effective are they? [Here, it is worth noting that short contacts between heteroatoms are defined by the sum of the van der Waals radii of the two participating atoms, such that a measured or calculated interatomic distance for a close contact is less than this value. A description of the various types of non-covalent bonding observed in acenes is nicely described by Sutton, Risko and Brédas,[5] whilst for heteroatom interactions there are numerous reviews describing intermolecular pnictogen,[6] chalcogen,[7]and halogen[8] interactions.] CT salts based on tetrachalcogenofulvalenes provide an excellent case study. The compound tetramethyltetraselenafulvalene (TMTSF) can be oxidized electrochemically using a range of electrolytes to give the family of CT salts, $(TMTSF)_2X$ (where X is an anion), known as the Bechgaard salts. As an example, the structure and packing of the donor molecule in $(TMTSF)_2NO_3$, obtained from X-ray diffraction studies at 125 K,[9] are shown in **Figure 1**.

Focusing on the packing of the donor TMTSF molecule, it can be seen that the molecules adopt a stacked structure with short contacts between adjacent stacks (Figure 1b). The sum of the van der Waals radii for two Se atoms is 3.80 Å,[10] meaning that the Se···Se contacts within the stacks (3.795 Å) and between stacks (3.616 and 3.766 Å), as shown in Figure 1c, give orbital overlap in two dimensions. The saturated methyl groups of the TMTSF molecule do not allow further heteroatom contacts in the third dimension (Figure 1d). The Bechgaard salts are well-known for their high levels of conductivity. Whilst the anions (X) do not affect the electronic properties of the salts and the crystals are

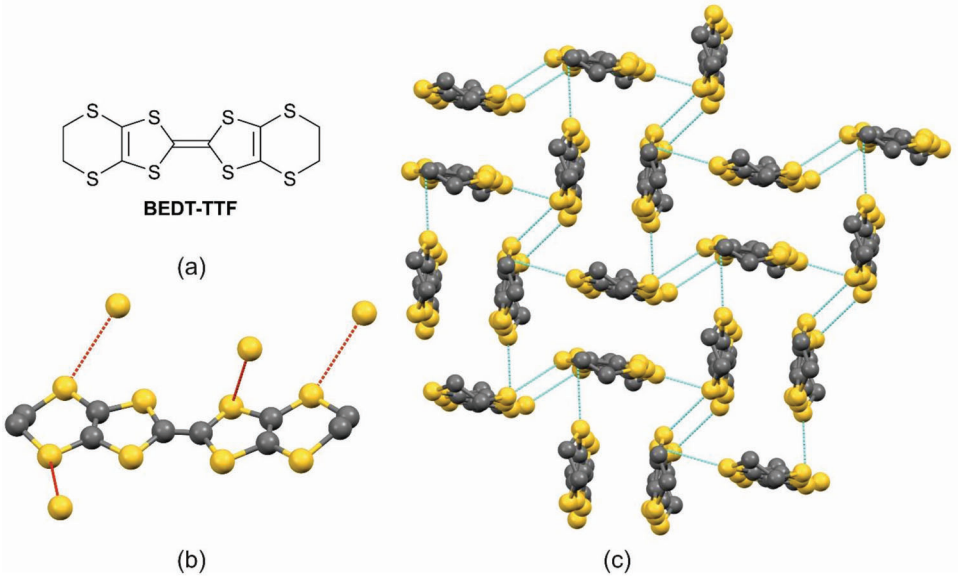

Figure 2. Structure and packing of BEDT-TTF in the CT salt $(BEDT\text{-}TTF)_2Cu[N(CN)_2]Br$: a) chemical structure; b) four sites of short S···S contacts arising from one molecule; c) κ-packing motif of the donor molecules showing intermolecular S···S contacts in two dimensions.

isostructural, the anions do have a varying effect on the packing of the TMTSF, specifically in terms of the Se···Se distances. The salts have metallic conductivity and become superconducting under pressure when the Se···Se networks contract (with the exception of $(TMTSF)_2ClO_4$, which is superconducting at ambient pressure).[11]

From a glance at the structures shown in Figure 1, one could argue that the electronic properties of the Bechgaard salts could be dominated by π-π stacking (ring-over-bond overlap is observed down the stacks with ring centroid to C (central C≐C) distances of 3.54 to 3.64 Å), but research has shown that the interstack interactions in the Bechgaard salts are key to their highly conducting behavior.[12] Further proof of the importance of heteroatom interactions can be seen from the structures of CT salts based on the molecule bis(ethylenedithio)tetrathiafulvalene, BEDT-TTF. The solid-state structure of the donor molecule in the salt $(BEDT\text{-}TTF)_2Cu[N(CN)_2]Br$ is shown in **Figure 2**.[13] Figure 2b shows the extensive nature of the S···S contacts observed in the structure, with four sets of interactions emanating from each molecule. The molecules are arranged in a 2D kappa-packing motif, in which the molecules assemble as face-to-face dimers with the dimers arranged orthogonally to each other (Figure 2c). In such a structure, π-π interactions are restricted to the dimers and are therefore very short range. The sum of the van der Waals radii for two sulfur atoms is 3.60 Å[10] and the S···S contacts are 3.150 Å between molecules in the same plane and 3.595 Å between orthogonal molecules. The CT material has a transition temperature for superconductivity of 11.6 K at ambient pressure. The long-range electronic interactions that give rise to these properties are derived entirely from orbital overlap between the sulfur atoms.

The above demonstrates the importance of heteroatom interactions in simple molecules designed for high levels of conductivity, but the same phenomenon can be exploited in the design of conjugated organic semiconductors. Higher dimensionality and even control of conformation[14] can be achieved through heteroatom interactions and these will be demonstrated in the next two sections.

3. Heteroatom Interactions in Molecular-Based Organic Semiconductors

Molecular-based organic semiconductors (OS) have a series of advantages over their polymeric counterparts. Being monodisperse systems, they are characterized by precise energy levels, originated from their well-defined structure. They can be obtained in a pure form by conventional methods of purification and their properties are 100% reproducible.[15] As we will see in this section, intramolecular heteroatom interactions define the planarity of the molecular conjugated backbone and provide a significant contribution to the energies of molecular frontier orbitals. In the solid state, the splitting of the HOMO and LUMO energy levels, which define the valence and conduction bands, respectively, heavily depends on the strength of intermolecular interaction. As mentioned in the previous section, the dimensionality of intermolecular interactions is very important, not only for organic metals, but for OS as well, as it defines how efficient charge transport is in different directions.[2] The efficiency of the most important intermolecular coupling, π-π stacking, on the other hand, heavily depends on the planarity of the molecular system, so this type of interaction can be affected by both intra- and intermolecular heteroatom coupling. As it was seen for synthetic metals in the previous section, the most informative way to study heteroatom interactions is by analyzing the single crystal diffraction data. For molecular-based OS this is the most reliable way to identify and analyze the heteroatom interactions.

Non-covalent interactions for conformational locks were reviewed in the recent paper by Huang et al.[16] In this section of the review we are going to focus our attention on materials for organic photonics and electronics where the structures were

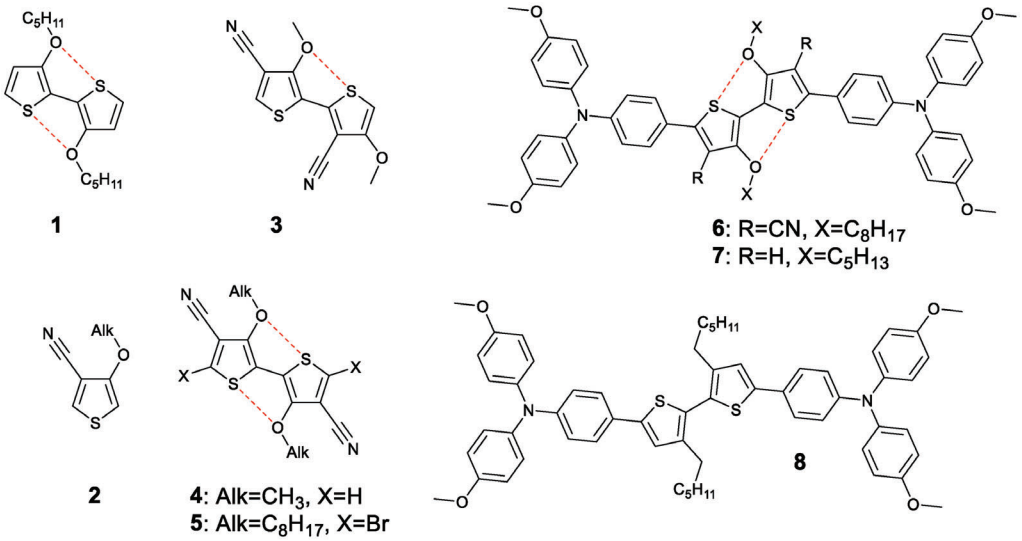

Figure 3. Compounds featuring bithiophene units with S···O conformational locks (1,3-7), thiophene 2, used for the synthesis of bithiophenes 3–5 and compounds 6–7 tested as HTMs for high performance inverted PVSCs.

resolved by X-ray crystallography, or the interactions were revealed through properties related to the materials applications.

3.1. S···O non-Covalent Interactions

The simplest way to introduce S···O conformational locks into oligothiophene architectures is to incorporate alkoxy substituents at the 3- and 3'-positions of the 2,2'-bithiophene unit. In 1994 Meille et al. analyzed the crystal structure of 3,3'-dipentyloxy-2,2'-bithiophene (1) and discovered S···O non covalent interactions (**Figure 3**).[17] Later, Roncali's team designed a convenient method for the synthesis of 4-alkoxy-thiophen-3-carbonitrile (2). The methoxy derivative 2 (Alk = CH_3) was used for the synthesis of 2,3'-dicyano-2',3-methoxythiophene (3). The crystal structure of compound 3 showed an efficient S···O conformational lock.[18] Using the corresponding derivatives of thiophene 2, Guo et al. synthesized the symmetric bithiophene 4, the crystal structure of which revealed S···O non-covalent interactions,[19] and bithiophene 5, which they used as a core for the synthesis of compound 6.[20] The latter, compound 6, revealed in a single crystal X-ray diffraction analysis short S···O contacts (2.92 Å) and a high degree of planarization of the bithiophene central unit which contributed to compact intermolecular π-π stacking with an interplane distance of 3.52 Å.[20] This efficient packing provided a high degree of crystallinity of the film and contributed to an increased intrinsic hole mobility of 6 (1.81×10^{-4} cm^2 V^{-1} s^{-1}) measured by the space-charge-limited current (SCLC) method. For a comparison of the effect of non-covalent interactions on the p-type behavior of this material, the authors synthesized the analogous compound 7 with pentyloxy groups but without CN functionality and compound 8 without S···O non-covalent interactions, functionalized with hexyl chains instead of pentyloxy groups in compound 7. Compound 7 showed an almost twofold lower mobility of 9.52×10^{-5} cm^2 V^{-1} s^{-1}, and compound 8, without S···O intramolecular non-covalent interactions, exhibited a significantly lower mobility of 3.65×10^{-5} cm^2 V^{-1} s^{-1}. The high film crystallinity of compound 6 and its increased hole mobility rendered this material as an efficient dopant-free hole-transporting material (HTM) for high-performance inverted perovskite solar cells (PVSCs) with a power conversion efficiency (PCE) of 21.1%, one of the highest values reported for dopant-free small molecule HTMs based on an inverted PVSC. Devices containing material 8, without S···O non-covalent interactions showed a significantly lower PCE of 18.4%.

Another structural motif which introduces the efficient S···O interactions into oligothiophene architectures is the 3,4-ethylenedioxythiophene (EDOT) unit. As can be seen from Section 4, this feature has made EDOT-based polymers one of the most popular p-type organic semiconductors. The crystal structure of the biEDOT molecule[21] reveals evidence of non-covalent S···O interactions (**Figure 4**). The biEDOT unit was featured in a series of molecular based organic semiconductors.[22] The Roncali group incorporated biEDOT as a spacer into push-pull chromophore 9, designed for application in second order nonlinear optics (NLO). The NLO properties of compound 9 was compared to those of the push-pull system 10 with the same donor and acceptor unit but different 2,2'-bithiophene spacer.[21] Compounds 9 and 10 were used for measuring the electric field induced second harmonic generation in $CHCl_3$. Incorporation of the biEDOT unit as a linker between (4-dimethylamino)styryl donor and 1,3-bis(dicyanomethylidene)indan-3-ylidenemethyl acceptor units led to a 118 nm red-shift in the absorption maximum of compound 9 (λ_{max} = 830 nm) compared to its bithiophene analogue 10 (λ_{max} = 712 nm) and a more than twofold increase in the quadratic hyperpolarizability of compound 9 ($\mu\beta$ = 11 600 × 10^{-48} esu) compared to compound 10 ($\mu\beta$ = 5000 × 10^{-48} esu). However, the dipole moment of compound 9 (μ = 17.1 D) is only slightly higher than that of 10 (μ = 15.9 D).[23] Therefore, the strong enhancement in quadratic hyperpolarizability cannot solely be explained by the increase in the dipole moment, confirming that the more than

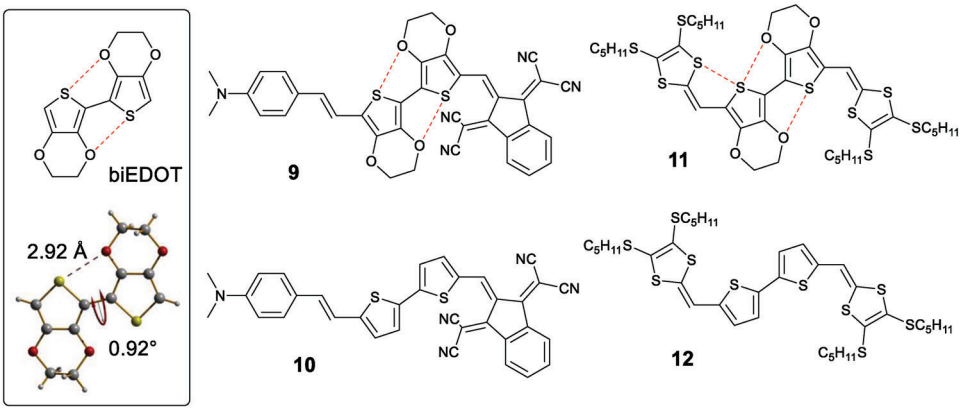

Figure 4. Conformational lock in the biEDOT molecule, compounds 9 and 11 featuring biEDOT units, and their analogue 10 and 12 with bithiophene as π-conjugated linker units.

twofold increase in $\mu\beta$ is due to rigidification of the biEDOT unit from the non-covalent S···O interactions, which makes biEDOT a much more efficient spacer than bithiophene in push-pull donor-acceptor systems for NLO applications.

The biEDOT unit was used as a conjugated spacer in extended TTF molecule 11.[24] The crystal structure of this compound (**Figure 5**) revealed not only the aforementioned intramolecular S···O non-covalent interactions within the biEDOT unit, with a dihedral angle between the two EDOT units less than 0.2°, but also intramolecular S···S non-covalent interactions with an interaction distance of less than 3.1 Å, which is less than the sum of the van der Waals radii of two sulfur atoms (3.60 Å). The displaced stacking interactions of the molecule in the crystal lattice, caused by steric hindrance, featured an intramolecular close contact of 3.58 Å between a sulfur atom of the dithiol ring in one molecule and another sulfur from an EDOT unit. The S···O intramolecular interaction is retained in solution which was confirmed by both UV-vis absorption and cyclic voltammetry (CV) measurements. The absorption spectrum of compound 11 exhibited a red shift compared to that of compound 12 due to the decrease in HOMO-LUMO gap, dictated by the more rigid conjugated backbone of 11, as well as more enhanced vibronic splitting compared to that of 12. Better conjugation between dithiolidene groups in the rigid molecule 11 provided the higher degree of HOMO

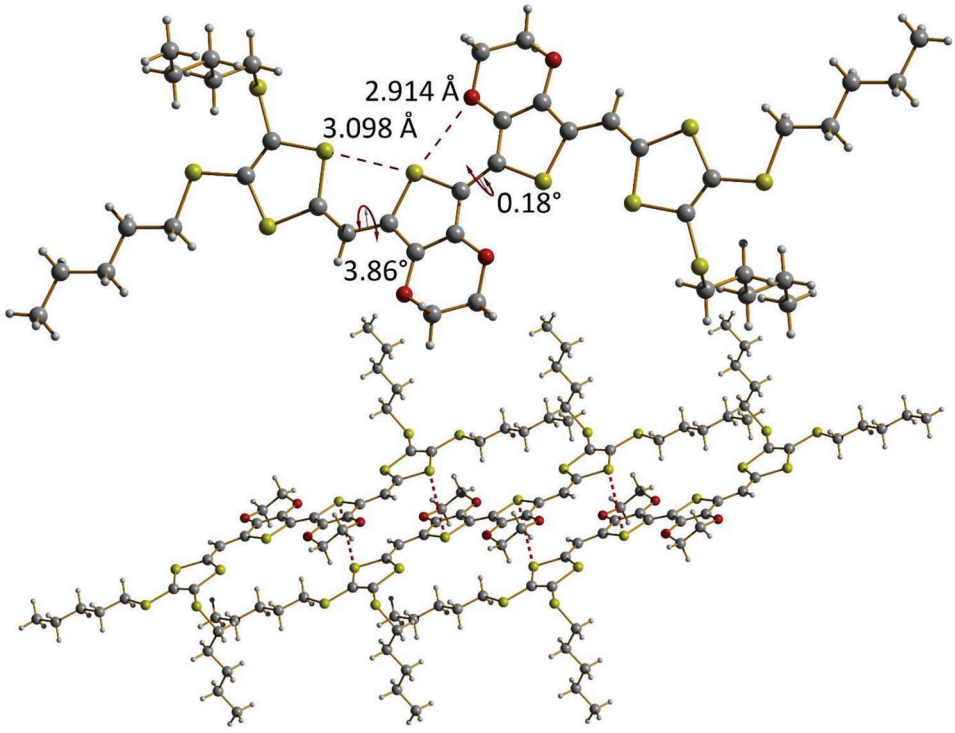

Figure 5. The non-covalent intramolecular interaction in the crystal structure of molecule 11 and intermolecular close contacts between the sulfur atom of the dithiol unit in one molecule and a sulfur of an EDOT unit in another (3.58 Å), shown by dotted lines.

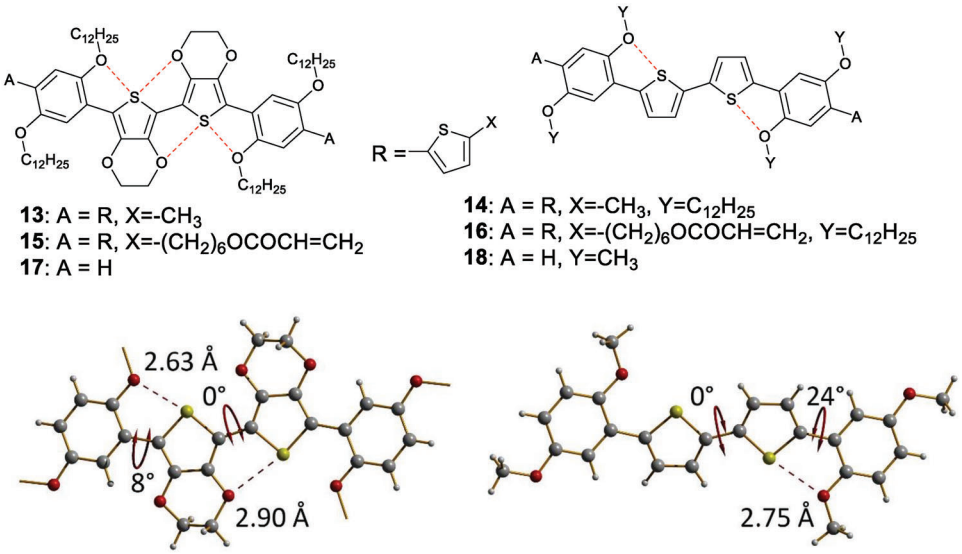

Figure 6. The structures of discrete cross-linkable photo-patternable materials 15 and 16 for photochromic applications; the model compounds 13 and 14 used for investigating electrochemical and optical properties of the structural motif used in the materials 15 and 16 and compounds 17 and 18, the crystal structures of which are shown below. In the case of compound 17, the dodecyl groups are omitted for clarity.

destabilization and stronger electrostatic repulsion between positive charges in the dication species compared to those of compound 12. These led to a decrease in the first oxidation potential (E_1) and an increase in ΔE (E_2-E_1) of 11 compared to those of 12, respectively.

Similar electrochemical behavior to that observed upon oxidation of 11 and 12 was reported by the Reynolds group for molecules 13 and 14, which were synthesized as model compounds for discrete cross-linkable photo-patternable materials 15 and 16, respectively (**Figure 6**).[25] The CV of both compounds 13 and 14 revealed two well-resolved oxidation waves corresponding to oxidation to the cation-radical and then dication. The first oxidation wave was lower for compound 13 ($E_{1/2,\,1ox}$ = 0.15 V versus Fc/Fc^+), featuring a biEDOT central unit, compared to that of compound 14 ($E_{1/2,\,1ox}$ = 0.24 V versus Fc/Fc^+), with a bithiophene central unit. The second oxidation wave was higher for compound 13 ($E_{1/2,\,1ox}$ = 0.50 V versus Fc/Fc^+) than for compound 14 ($E_{1/2,\,1ox}$ = 0.45 V versus Fc/Fc^+). This trend confirmed that rigidification of the biEDOT unit due to non-covalent interactions takes place in solution. The non-covalent S···O locking in crystals was confirmed by single crystal X-ray diffraction studies of other model compounds (17 and 18). Although in the crystal the central bithiophene unit of 18 is planar, this planarity is not preserved in solution. The authors observed a broad and featureless absorption for compound 13, while the spectrum of compound 14 showed vibronic features attributed to the S···O non-covalent interactions within this molecule. In an electrochromic device, compound 15 showed much higher current response and stability of the doped state compared not only to compound 16 but also to a similar photochromic material featured with a sexithiophene conjugated backbone.

The biEDOT unit was also incorporated into a π-extended bipyranylidene conjugated system 19 for electron doping of n-type organic thermoelectric materials (**Figure 7**).[26] The single crystal structure of 19 revealed a greater degree of planarity due to the extended biEDOT core with non-covalent S···O interactions, compared to the structure of 20. Although the electrochemically estimated HOMO energy level for compound 19 (−4.41 eV) was only slightly higher, relative to vacuum, than those of compound 20 (−4.44 eV) and 21 (−4.52 eV), the work function determined by Kelvin probe for the thin film of 19 (−3.94 eV) was significantly lower than those of 20 (−4.20 eV)

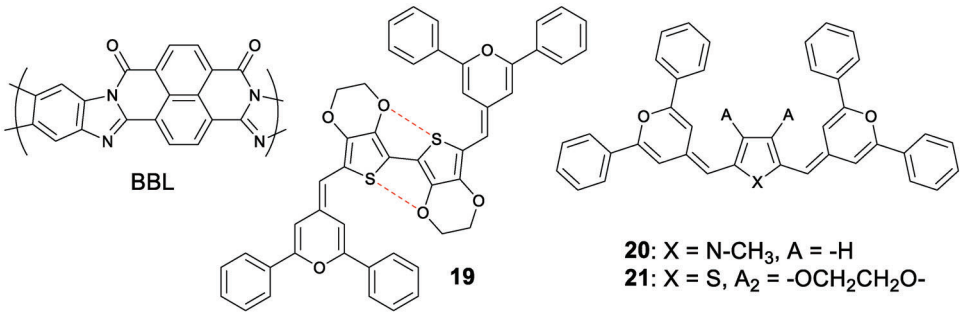

Figure 7. The structure of *n*-type semiconductor polymer BBL and the donor molecules 19–21 used for n-doping.

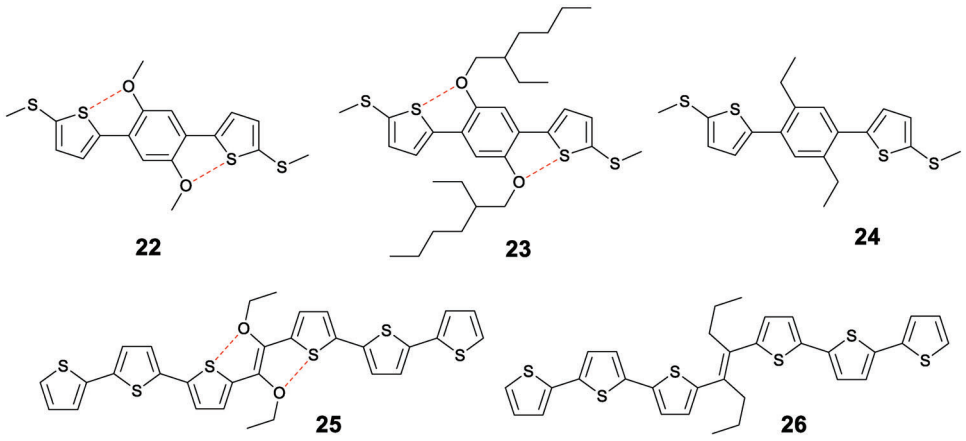

Figure 8. The structures of molecules 22–24 used for the study of the effect of non-covalent interactions on single molecule conductivity and the oligothiophenes 25, 26 with substituents at the vinylene linkage.

and 21 (−4.16 eV), which contributed to a better performance of material 19 compared to 20 and 21. The electron doping of poly(benzimidazobenzophenanthroline) (BBL) by 19 resulted in good thermoelectric characteristics of the doped BBL film with a power factor of 1.25×10^{-3} μW m^{-1} K^{-1}, one order of magnitude higher than those for the BBL films doped with compounds 20 and 21 (**Figure 7**).

The effect of S···O non-covalent interactions on the conductivity of single molecules with methylthio anchor groups and a di(thiophen-2-yl)benzene conjugated backbone was studied using compounds 22 and 23, systems with S···O conformational locks, as well an analogous molecule (24) without intramolecular non-covalent interactions (**Figure 8**).[27] The crystal structure of 22 revealed a S···O distance of 2.707 Å and a dihedral angle between thiophene and benzene rings of only 1.7°. Compound 23, which had bulky alkoxy substituents, exhibited a similar S···O interaction distance of 2.742 Å but had a higher dihedral angle of 20.1°. The crystal structure of compound 24 on the other hand showed the highest dihedral angle of 52.1°. The molecular conductance of compounds 22 ($\approx 10^{-3.30}$ G_0), 23 ($\approx 10^{-4.10}$ G_0), and 24 ($\approx 10^{-4.19}$ G_0) measured at 0.1 V follows a trend of the change in planarity for these compounds, confirming the strong influence of conjugation on single molecule conductance. The measurements at an increased voltage of 0.5 V showed no apparent change in molecular conductance for compounds 22 and 24 but led to a significant increase in the conductance of 23 ($\approx 10^{-3.17}$ G_0), with a 2D conductance histogram confirming the same length of ≈ 1.4 nm for compounds 22–24 at different applied biases (0.1 and 0.5 V). The authors drew the conclusions that the large modulation of the molecular conductance for compound 23 with bulky substituents is due to a change in the molecule's planarity at elevated voltage and suggested that molecules with S···O intramolecular interactions can be used as molecular switches.

Another way to incorporate solubilizing alkoxy groups and providing S···O non-covalent interactions within the π-conjugated backbone of an oligothiophene system is via a vinylene linkage. In this case, the HOMO energy level would not rise as high as for the system with alkoxy groups attached directly to the thiophene rings and the system would remain electron-neutral. An example of such an approach was given by the Facchetti group who compared the properties of molecular based OS 25 to that of 26 (Figure 8).[28] The more planar structure of compound 25 due to S···O non-covalent interactions provided a smaller HOMO/LUMO energy gap (−5.4/−3.5 eV) compared to that of 26 (−5.4/−3.1 eV) by lowering the LUMO level. The field-effect hole mobility of oligomer 25 was 3×10^{-3} cm^2 V^{-1} s^{-1}, while the compound 26 didn't show any field-effect activity.

An unusual effect of S···O non-covalent interactions on the optical properties of (E)-1,2-bis(hetaryl)ethene compounds 27–32 was reported by the Huang group.[29]

Compounds without substituents at the ethylene bridge (27, 28, and 31) were found to show common aggregation caused quenching (ACQ), while their diethoxy substituted analogues (29, 30, and 32) exhibited unusual aggregation-induced emission (AIE). The authors investigated the crystal structures of 31 and 32 in order to shed a light on the strange behavior of 32. The single crystal X-ray diffraction study of 31 revealed a fairly planar structure (**Figure 9**). The close packing in the $P2_1/c$ space group led to weakening of the fluorescence of this compound in the solid state with a photoluminescence quantum yield (PLQY) of 4.7% as opposed to 13% in THF solution, which is normal ACQ behavior. Despite the presence of ethoxy groups, the planarity of the

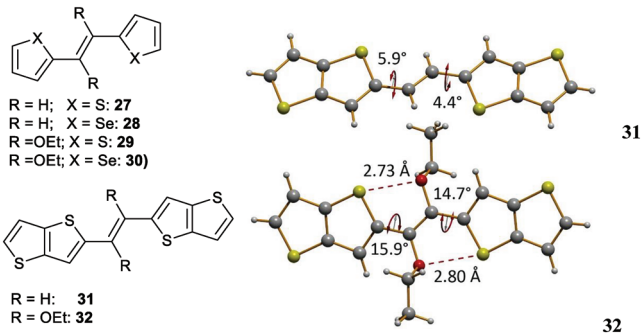

Figure 9. Compounds (27-32) used for comparison of fluorescence in the solid state and in solution, and the crystal structures of compounds 31 and 32.

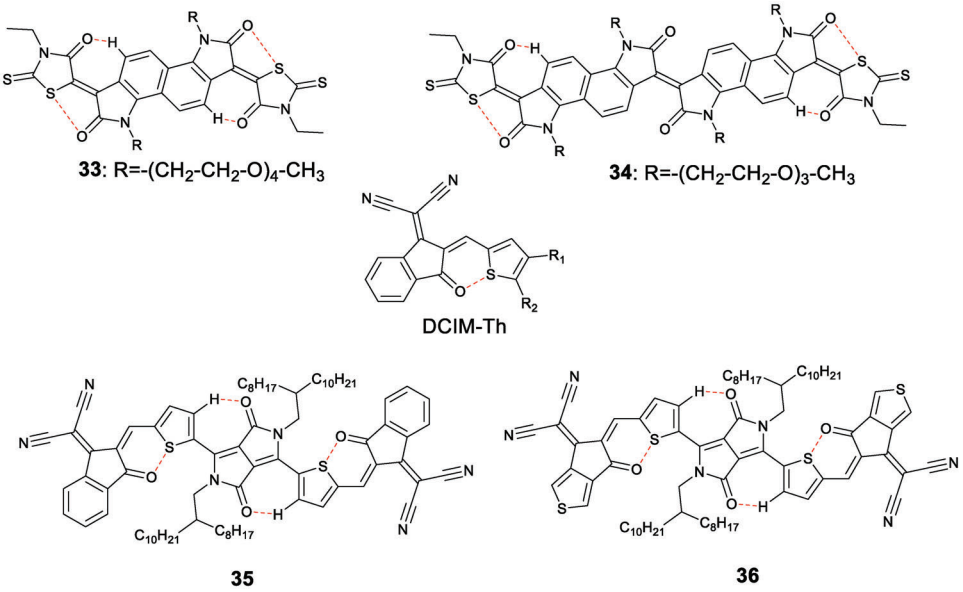

Figure 10. Compounds (34) used for application in OECT, and *n*-type organic semiconductors featuring DCIM-Th units (35-36).

bis(thienothiophene)ethene conjugated backbone is retained in the crystal structure of 32 due to non-covalent S···O interactions with a distance between sulfur and oxygen atoms in the range 2.7–2.8 Å, which is shorter than the sum of the van der Waals radii of the two atoms (3.25 Å). The crystal packing of 32 also revealed intermolecular C–H···O hydrogen bonding with interaction distances of ≈2.7 Å between oxygen and hydrogen atoms of the ethoxy groups, which makes crystal packing more rigid, hinders π-π interaction and decreases the rate of non-radiative decay in the solid state. Despite the heavy atom effect, the PLQY of a powder sample of 32 was found to be 5%, while the crystal sample exhibited a stronger luminescence with a PLQY of 17%. In contrast to the solid-state luminescence, the samples of 32 in THF solution exhibit almost no fluorescence (PLQY = 0.13%). The authors explained unusual fluorescence quenching in solutions of 32 by trans-cis photo-isomerization facilitated by the non-covalent S···O interactions.

The conformational lock strategy has been used recently to provide the best degree of planarity for organic molecular based acceptors designed for n-type organic electrochemical transistor (OECT) applications (**Figure 10**).[30] For these compounds, the S···O and O···H–C non-covalent interactions between the rhodanine and isatin units were evidenced by density functional theory (DFT) calculations.[30a,c] Due to a high degree of crystallinity provided by the π-acceptor's planarity, compounds 33 and 34 have shown the best μC* figures of merits of 5.12[30b] and 10.3 F cm^{-1} V^{-1} s^{-1},[30c] respectively.

S···O non-covalent interactions are involved in providing the maximum conjugation between donor and acceptor moieties in small molecule donor acceptor systems. The most common motif of this type is based on the 3-dicyanomethylideneindan-1-one-2-ylidenemethyl acceptor group (DCIM) coupled to a thiophene (Th) unit, which normally reveals S···O non-covalent interactions between the carbonyl oxygen and thiophene sulfur atoms. This type of conformational lock was featured in the symmetrical molecules comprising the 1,4-dioxa-2,5-dialkyl-3,6-di(thiophen-2-yl)-pyrrolo[3,4-c]pyrrole (ThDPP) central unit and DCIM groups (35) or its thieno-analogue acceptor units (36) (Figure 10). Compounds 35 and 36 were used for the design of *n*-type organic semiconductors with an increased electron mobility and showed maximum electron mobilities of 0.18 and 0.77 cm^2 V^{-1} s^{-1}, respectively.[31]

The crystal structure of 35 (**Figure 11**) revealed a planar centrosymmetric molecule in the lattice of a triclinic space group with strong intramolecular S···O interactions between the carbonyl oxygen of the 3-dicyanomethylideneindan-1-one-2-methylidene unit and the sulfur atom of thiophene, with an interaction distance of 2.70 Å. Due to this interaction, the dihedral angle around the bond connecting the aforementioned acceptor unit and the thiophene ring is only 2.72°. The hydrogen bond between the DPP carbonyl oxygen atom and the H-atom of thiophene is responsible for a small dihedral angle of 4.97° between the central DPP and thiophene units. The crystal lattice reveals close packing with the distance between the parallel planes of the molecules of 3.6 Å.

The crystal structure of compound 36 (**Figure 12**), which showed better OFET performance, is similar to that of 35.

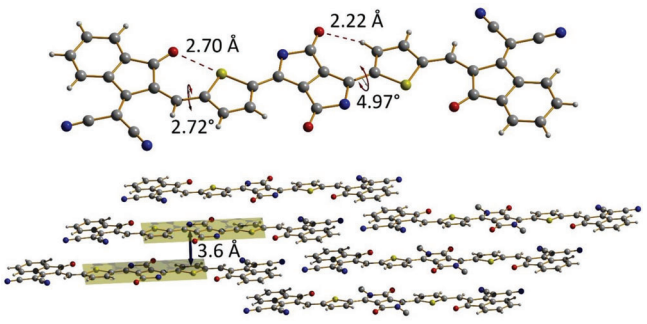

Figure 11. The crystal structure of 35 (top) and the packing of the molecules in the crystal lattice (bottom).

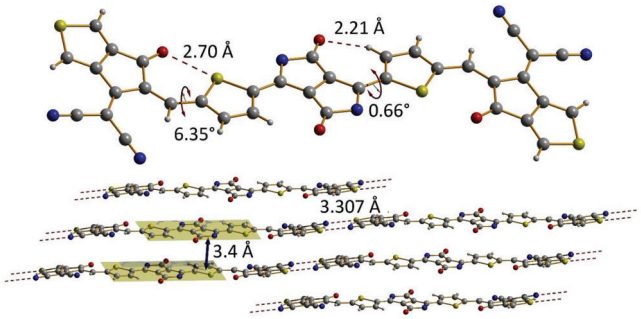

Figure 12. The crystal structure of 36 (top) and the packing of the molecules in the crystal lattice showing infinite S···N contacts between molecules in the same plane (bottom).

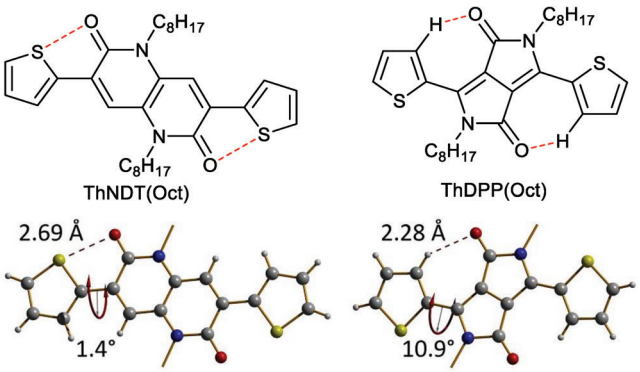

Figure 13. The crystal structures of the two different centrosymmetric bis-lactam acceptor molecules, with S···O non-covalent interactions in ThNDT(Oct) and the O···H hydrogen bonding in ThDPP(Oct) controlling the planarity of the conjugated backbones. The octyl chains are omitted for clarity.

Interestingly, in this case despite displaying very similar S···N and O···H interaction distances of 2.70 and 2.21 Å, respectively, the dihedral angle between the terminal acceptor and thiophene units is notably higher (6.35°) and the angle between central DPP and thiophene units is lower (0.66°), compared to those of 35. The packing pattern displays a lower inter-plane distance of 3.4 Å. Close examination of the packing reveals infinite chains of N···S close contacts (3.307 A), which can be responsible for the aforementioned differences.

The HOMO/LUMO levels estimated by CV were found to be −5.58/−3.99 and −5.65/−4.05 eV for 35 and 36, respectively. The lower LUMO level of 36 compared to that of 35 and its closer packing pattern is consistent with the higher electron mobility exhibited by this material. The authors mentioned that there is red-shifted absorption for both materials in the solid film compared to those in solution, which is due to intermolecular interactions of quadrupolar molecular systems in a condensed phase.[32]

As can be seen from the structures of 35 and 36, the conformation of the central ThDPP unit is dictated by hydrogen bonding. This unit has been extensively used for the design of both donor and acceptor materials for organic photovoltaic devices (OPVs).[33] Another bis-lactam acceptor developed by the Park group showed, in the crystal structure, the dominating S···O non-covalent interactions which provide planarity of the molecule (**Figure** 13).[34] A comparison of the optical properties of ThNTD and ThDPP showed that the former has a higher absorption coefficient ($\epsilon = 4.07 \times 10^4$ L mol^{-1} cm^{-1}), PLQY ($\Phi = 0.98$) and lower fluorescence lifetime ($\tau = 3.33$ ns) compared to ThDPP ($\epsilon = 2.93 \times 10^4$ L mol^{-1} cm^{-1}, $\Phi = 0.85$, $\tau = 6.15$ ns). The high absorption coefficient and PLQY of ThNTD make this structure a useful building block for the design of fluorescent 2,3 biomarkers.[35]

The aforementioned DCIM-Th unit has been featured in numerous electron-deficient systems which have been applied as non-fullerene acceptor (NFA) components for organic solar cells. Since the report of ITIC, the first A-D-A type of electron-deficient system,[36] followed by the application of Y6, an A-DAD-A type of NFA for OPVs,[37] it has been realized that the narrow band gap, fused polycyclic materials can not only outcompete fullerenes but open a real prospect for the practical application of OPVs. The crystal structures of all efficient non-fullerene acceptors show an efficient S···O non covalent interaction within the DCIM-Th unit.[38] The advantage of the efficient S···O conformation lock can be illustrated by a recent report on extending the fused ring donor unit of the A-D-A type acceptor from a heptacyclic unit in BTPIC-4F to a nonacyclic one in TTPIC-4F (**Figure** 14).[39] The more efficient intramolecular non-covalent interactions between the carbonyl oxygen atom of peripheral acceptor groups and the terminal thiophene sulfur atoms of the central donor unit was revealed by the crystal structure of TTPIC-4F. These interactions, along with a more extended donor core unit, led to a more planar molecule, which provided the possibility for a lower reorganization energy[40] and resulted in more efficient π-π stacking interactions, higher crystallinity and lower density of trapped states compared to its non-extended analogue BTPIC-4F.[39] This led to a higher PCE exhibited by the D18:TTPIC-4F based device (17.1%, the highest PCE shown by an A-D-A type acceptor), compared to that of D18:BTPIC-4F (10.3%).

The multistep synthesis of a multi-ring fused system of the most efficient NFAs is a serious obstacle on the way to their practical applications. However, the S···O conformational lock has been used to simplify the structure of A-D-A NFAs. The crystal structure of FOC2C6-2FIC and FOC6-IC revealed both S···O and S···F intramolecular interactions involved in the conformational lock of the central donor units.[41]

3.2. S···N non-Covalent Interactions

In the case of S···N non-covalent interactions, the most efficient way to introduce the conformational lock is to incorporate a N-containing heterocycle into the conjugated backbone of an oligothiophene to enhance planarity of the conjugated system and to seed intermolecular interactions into the bulk of a molecular-based OS. The most popular choice of the heterocyclic unit is thiazole itself or in its fused form. One of the interesting examples of such an approach can be seen in the structure of 2,6-bis(4-hexylthien-2-yl)benzo[1,2-d:4,5-d']bisthiazole (37, **Figure 15**).[4] The crystal lattice of this compound revealed two centrosymmetric molecules with a series of non-covalent interactions. The intramolecular S···N interactions with close contacts of 3.07 and 2.98 Å in these molecules (sum of van der Waals radii of S + N is 3.35 Å), led to a high degree of planarity of the

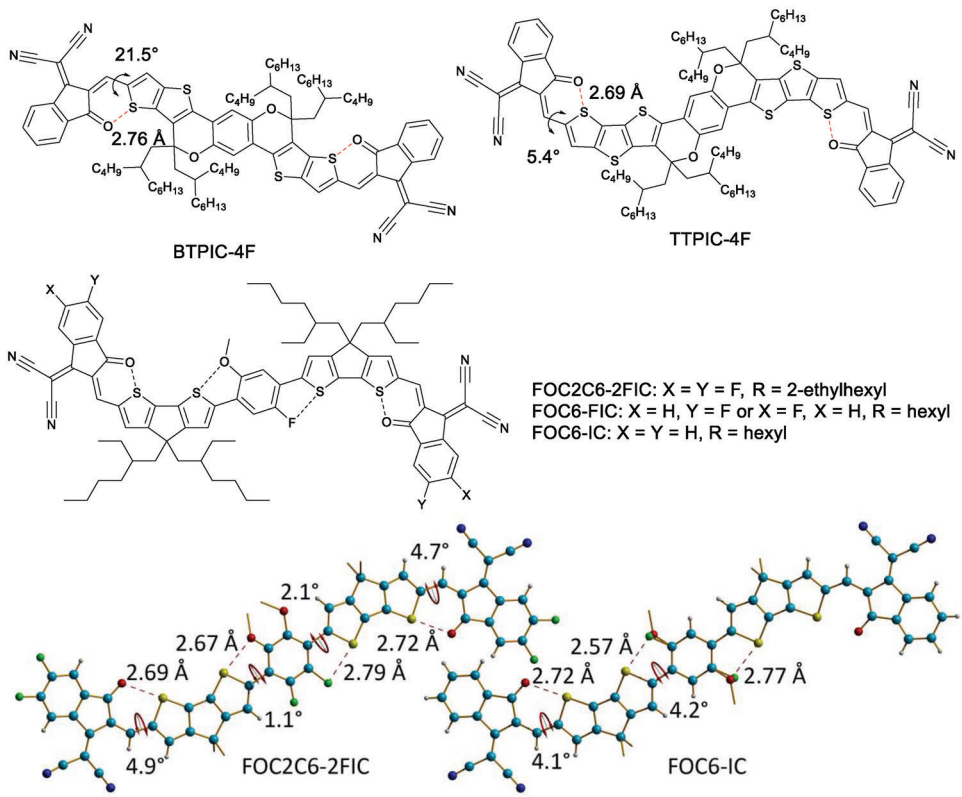

Figure 14. The structure of BTPIC-4F and TTPIC-4F, NFA featuring the S···O conformational lock between the peripheral acceptor groups and the central donor unit. The S···O interaction distances as well as dihedral angle values are given on the basis of the single crystal X-ray analysis. The structures of non-fused NFAs featured conformational locks within the central donor unit (the alkyl chains are omitted for clarity).

conjugated backbone with dihedral angles around bonds joining the benzo[1,2-d:4,5-d']bisthiazole (BBT) and thiophene heterocyclic units of 1.3° and 0.14° (Figure 15a). The intermolecular S···N close contacts of 3.02 Å form an infinite supramolecular chain network (Figure 15b) and assists in nearly orthogonal orientation of the molecular planes (≈86 °) creating 2D π-π stacking interactions (Figure 15c). The S···N close contacts provide orbital overlap in a third dimension and the resulting arrangement of molecules in the crystal state provides a rare example of an organic semiconductor with intermolecular close contacts in 3D. These multidimensional intermolecular interactions could lead to efficient charge carrier transport across the bulk of organic semiconductor. Non-optimized OFET devices fabricated from this material with significant energy barriers between the contacts and semiconductor exhibited a hole mobility as high as 10^{-2} cm^2 V^{-1} s^{-1}.

The thiazole unit has been incorporated instead of thiophene into the analogous structures of hybrid terthiophene TTF systems 38[42] and 39[43] yielding compound 40 (**Figure 16**). The DFT calculations of related structures 41–43[42] with methyl groups instead of hexyl substituents revealed a more planar structure for the conjugated system 43, compared to those of 41 and 42.

Introducing thiophene units at the 4- and 7- positions of 2,1,3-benzothiadiazole (BT) and 2,1,3-benzooxadiazole (BO) implements both S···N and N···H hydrogen bonding interactions. These type of structure units have been used for the design of donor materials for bulk heterojunction OPVs with $PC_{61}BM$ as the acceptor. The structures of compounds 44 and 45 (Figure 16) showed disorder with small twist angles between thiophenes and the central acceptor BO/BT unit (14° for one thiophene and 18°/19° for the other). The thiophene-benzofuran units are more planar with a torsion angle of 6–8°. The distances between donor thiophene-benzofuran units are very similar for both compounds (3.43 Å for 44 and 3.46-3.47 Å), which is consistent with the similar averaged field-effect hole mobility shown by 44 (1.9×10^{-5} cm^2 V^{-1} s^{-1}) and 45 (1.7×10^{-5} cm^2 V^{-1} s^{-1}). In contrast to the OFET data, the performance of the OPV was significantly different with the BO core compound 44, showing a higher PCE of 2.6% compared to that of 45 (0.3%) due to significantly higher short circuit current density (*J*sc) of devices fabricated from 44. The improved morphology of the 44:PCBM blend was the main reason for its enhanced performance in OPVs.

Another possibility for enhancement of both S···N and hydrogen bonding interactions was realized in the structures of a series of benzobis(thiadiazole) core compounds 46a-f (Figure 16).[44] These compounds were studied by single crystal X-ray analysis and the results of the structural analyses were used to simulate charge carrier mobility. The most twisted structure was shown by the *o*-trifluoromethyl derivative 46c. The most promising material for OFET fabrication was found to be compound 46e with a *m*-trifluoromethoxy substitution pattern.

Another way to boost S···N interactions is to substitute one of the ≐CH– sites of the BT unit with nitrogen. This was done by incorporating the [1,2,5]thiadiazolo[3,4-c]pyridine (PT) unit into an

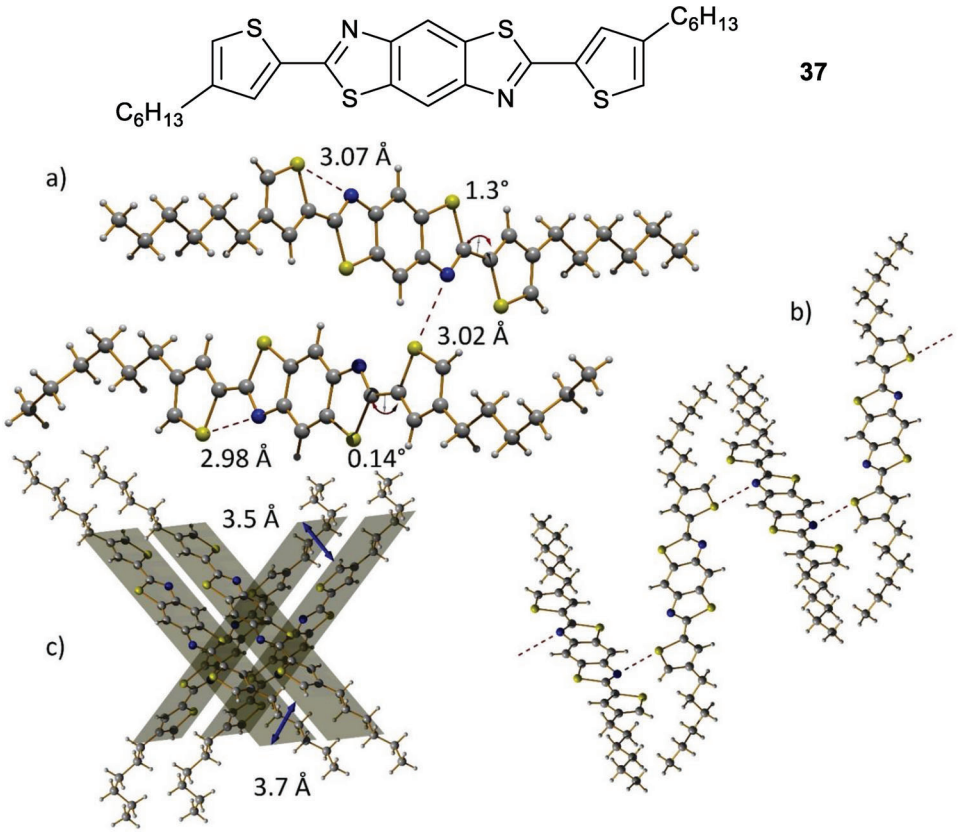

Figure 15. The molecular a) and crystal structures b,c) of 2,6-bis(4-hexylthiophen-2-yl)benzo[1,2-d:4,5-d']bisthiazole 37 revealing intra- and intermolecular S···N interactions in the two centrosymmetric molecules of the unit cell (a), the infinite chain of intermolecular S···N interactions (b), and stacking interactions in almost orthogonal directions.

oligothiophene. Takacs et al. performed a detailed study on the effect of S···N non-covalent interactions introduced in different isomers, 47a–47c, with D-A-D-A-D structure. These molecules all contained the PT acceptor, a central 3,3'-di-2-ethylhexylsilylene-2,2'-bithiophene and peripheral 2-hexylbithiophene donor units (**Figure 17**).[45] The analogous compound 48 with BT acceptor units was used as a reference material. Compounds with S···N conformational locks showed improved performance in OFETs with field-effect mobility values of 0.20, 0.07, 0.05, and 0.01 $cm^2\ V^{-1}\ s^{-1}$ for 47a–47c and 48, respectively. A similar trend of performance was observed for bulk heterojunction solar cells (BHJSCs), with these compounds used as donor materials along with $PC_{71}BM$ as an acceptor. The best PCEs recorded were 7.00, 5.56, 3.16, and 0.19% for 47a–47c and 48, respectively. The structure of the best performing material was resolved by single crystal X-ray analysis[46] and explicitly showed S···N non covalent interactions (distance of 2.9 A) which created a high degree of planarity of the conjugated backbone. To evaluate the impact of the S···N conformational lock on the structure of the molecule and the resulting properties, two isomers 49a and 49b with the same PT acceptor and central donor units but with the peripheral benzofuran moieties, have been investigated.[47] The molecular structure of compound 49a, featuring the S···N conformational lock, showed a higher degree of planarity compared to that of compound 49b. The absorption spectrum of compound 49a in chloroform solution showed distinct vibronic splitting, while the absorption band of 49b was featureless, confirming that the conformational S···N lock is retained in the solution of 49a. The spectra of the films spin-coated from chlorobenzene solutions of 49a and 49b are red-shifted compared to the corresponding spectra in solution and exhibit pronounced vibronic features due to the conformational constraints contributing to a planar structure of both 49a and 49b in the solid. The degree of bending has been estimated by measuring the angle between the lines connecting the Si bridge atom and two centroids of pyridine rings and found to be different for molecules 49a and 49b. The lower bending angle of 112.0° for 49a compared to that for 49b (116.1°) was explained by attractive S···N non-covalent interactions.

The PT acceptor unit was featured in the structure of the molecular-based emitter 50 for near-IR OLEDs (**Figure 18**).[48] The structure of compound 50 revealed a weak S···N interaction. However, the dihedral angle provided by this S···N contact is even higher than the one from the other side of the PT core unit and the fairly planar conformation of molecule 50 is likely to be controlled by hydrogen bonding and crystal packing (Figure 18a). The molecules are packed in a parallel manner with the distance between planes of the PT unit determined to be 3.6 nm (Figure 18b). The two stacks of the molecules are positioned in a face-to-face orientation in order to minimize the dipole–dipole interactions (Figure 18c). Absorption and emission spectra of

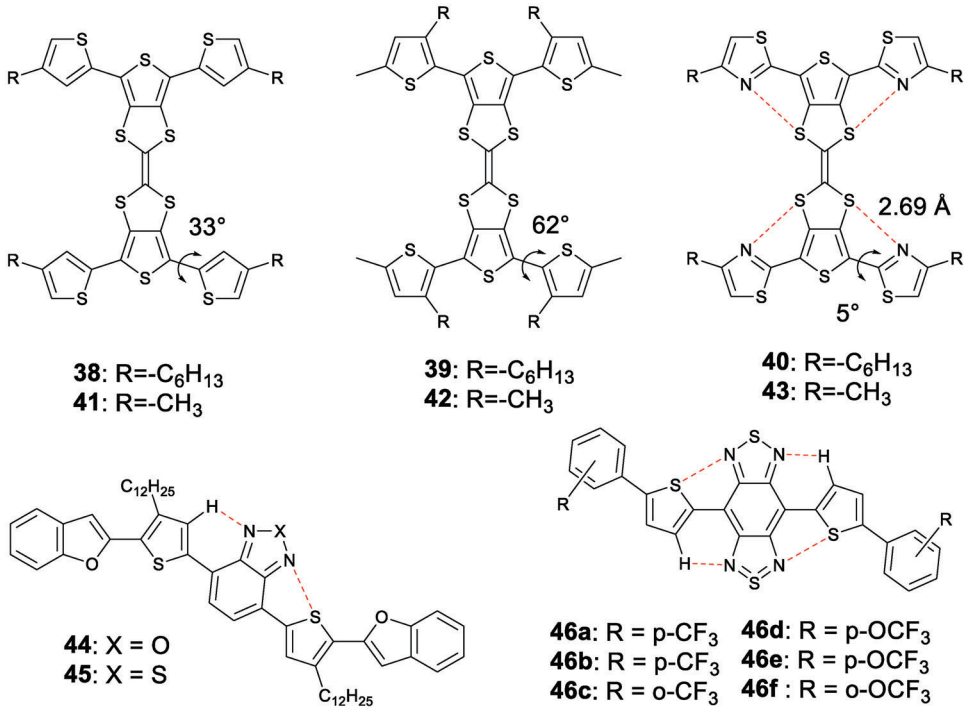

Figure 16. The structure of oligothiophene-TTF hybrid compounds 38–40. The values of dihedral angles as well as the S···N interaction distance for compounds with a thiazole unit are estimated by DFT structure optimisation of the corresponding structures 41–43 with methyl substituents. The donor materials 44–45 for bulk heterojunction solar cells (BHJSCs) featuring Th-BO-Th (44) and Th-BT-Th (45) units.

compound 50 both in solution and film did not reveal any vibronic features. The spectra in the film were red-shifted, compared to those in solution which might be due to dipole–dipole interactions in the solid phase.[49] The near-IR OLED fabricated from pristine material 50 showed emission at 816 nm, with a maximum radiance of 644 mW Sr^{-1} m^{-2} and a low turn on voltage of 3.3 V. Optimization of the device by using Alq_3 as a host material and compound 50 as a dopant allowed to shift the peak emission up to 848 nm and increase the maximum radiance of 2200 mW Sr^{-1} m^{-2} at 40% dopant concentration.

There is also an example of a near-IR emitter which features the [1,2,5]thiadiazolo[3,4-d]pyridazine (PzT) heterocyclic

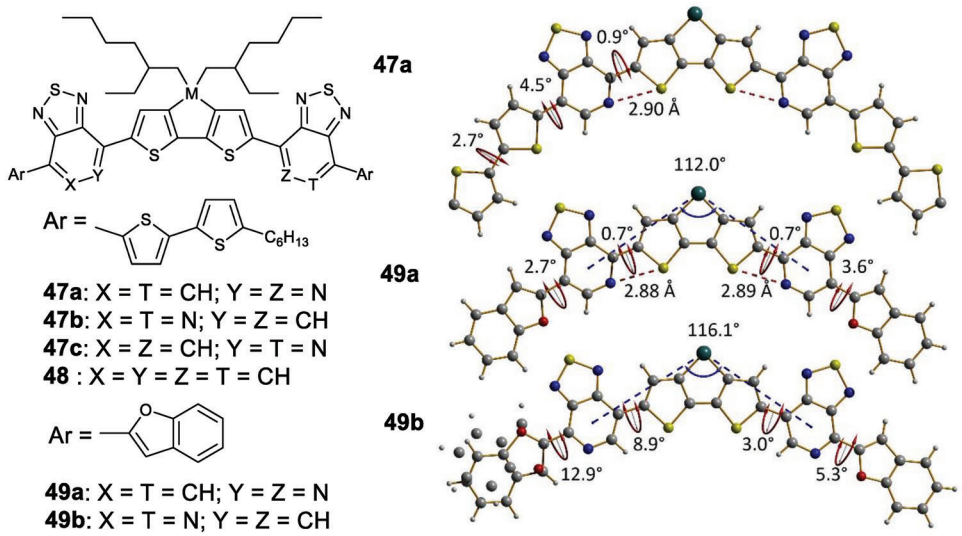

Figure 17. The D-A-D-A-D molecular systems featuring [1,2,5]thiadiazolo[3,4-c]pyridine (PT) as an acceptor with terminal bithiophene units 47a-47c and their 2,1,3-benzothiadiazole (BT) analogue 48, as well as two similar systems with terminal benzofuran units 49a-49b (alkyl chains in the structures of 47a, 49a, and 49b are omitted for clarity).

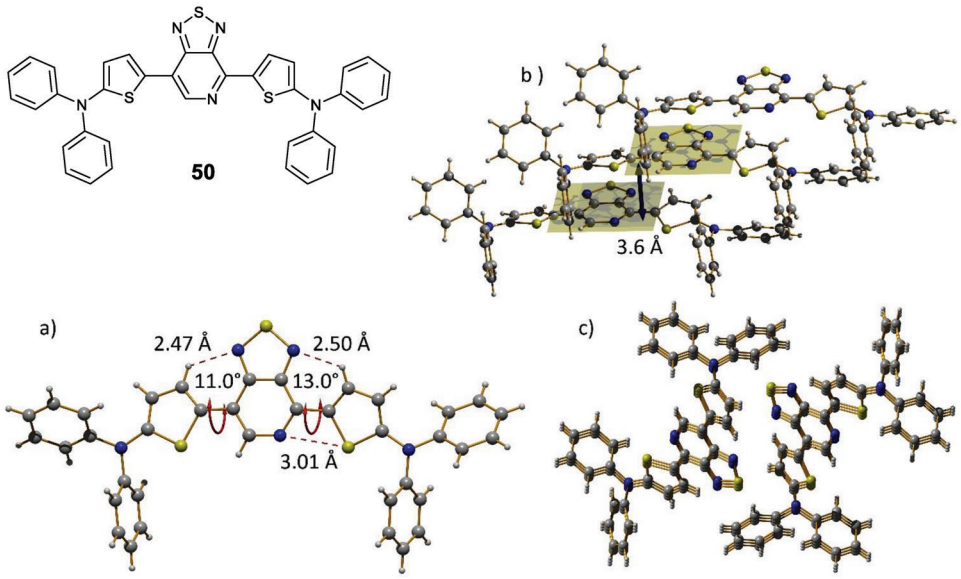

Figure 18. The D-A-D molecular system 50 featuring [1,2,5]thiadiazolo[3,4-c]pyridine (PT) as an acceptor, its molecular structure a), parallel packing in crystal b), and the view down two columns of stacked molecules along the *a* axis.

unit with potential S···N conformational locks.[50] Single crystal X-ray analysis revealed the asymmetric molecular structure of compound 51, which was explained by the packing effect (**Figure 19**). The molecules are packed in an antiparallel manner with a distance of 3.3 nm between the planes of the PzT unit. This type of close packing for compound 51 does not result in efficient luminescence and the near-IR OLED with $Be(bq)_2$ host doped with emitter 51 showed a maximum optical power of only 12 μW cm^{-2} at 157 mA cm^{-2}, corresponding to an EQE of 0.2%.

3.3. S···X non-Covalent Interactions

The S···F conformational lock was first demonstrated in 2001 when the crystal structure of perfluorosexithiophene 52 was reported.[51] The single crystal X-ray analysis revealed a high degree of planarity of the centrosymmetric molecule 52, with inter-ring dihedral angles of only a few degrees (**Figure 20**a). The molecular structure showed S···F non-covalent interactions with S···F distances lower than the sum of van der Waals radii. The high degree of planarity caused efficient packing of the molecules into a herringbone type of structure with $P2_1/c$ symmetry and alternating columns almost orthogonal to each other (84.7°, Figure 20b). Since then, S···F conformational locks have been actively used for conjugated polymers, which will be discussed in Section 4. As for molecular-based systems, these interactions have been applied in the design of NFAs by alternating 5,6-difluoro-2,1,3-benzothiadazole and s-indaceno[1,2-b:5,6-b']dithiophene units in the structure of IDBF-IC-n (n = 1-3) (Figure 20c).[52] The compounds with S···F conformational locks IDBF-IC-1, IDBF-IC-2 and IDBF-IC-3, showed higher PCEs of 12.1%, 4.8% and 1.4% in BHJSCs fabricated from their blend with the polymer donor PM6, compared to their analogues with non-fluorinated BT units IDB-IC-1 (10.3%), IDB-IC-2 (1.1%) and IDB-IC-3 (0.23%). As highlighted in Section 3.1 the structure of the two NFAs (FOC2C6-2FIC and FOC6-IC) featured S···F intramolecular interactions within the central donor unit which contributed to the planarity of the molecules (Figure 14).

Compounds 53–55 (Figure 20c) were used for the study of single molecule conductance using the STM-based break-junction method.[53] The statistical analysis of conductance-displacement (G-D) traces revealed high G_h and low G_l conductance peaks for each compound, which were ascribed to the states with Au tips bound to the π-plane of thiophenes and to their S atoms, respectively. Despite the increase in the tunnelling barrier between HOMOs and the Fermi level (E_F) (-4.6 eV), due to the lowering of HOMO levels with increased fluorine content (53 (−5.52 eV) > 54 (−5.60 eV) > 55 (−5.63 eV)), the conductance of the G_l state increased with the values 53 (2.18×10^{-5} G_0) < 54 (3.39×10^{-5} G_0) < 55 (8.71×10^{-5} G_0). The optimization of the structures showed S···F conformational locks for compounds 54 and 55 (Figure 20c). On the basis of experimental results and calculations, the authors assumed that the observed increase in conductance was due to an increase in planarity of the molecule as well as a through the space channel involving S···F intramolecular contacts.

S···F intermolecular interactions can cause supramolecular organization of molecular based organic semiconductors and control their bulk properties. Even minor alterations in the structures of fluorinated organic materials can lead to a significant change in the supramolecular organization of the molecules in the crystal state. An example of such an effect was shown in the crystal structure of fluorinated benzobisbenzothiophene.[54] Octafluorobenzobisbenzothiophene 56 crystallizes in monoclinic crystal with $P2_1/c$ symmetry with herringbone packing stabilized by a network of close S···F contacts, shown by the red dashed lines, with a length of 3.16 Å (**Figure 21**a).

The distance between the planes of the adjacent molecules in each column was found to be 3.36 Å, with the angle of 84.8° between the planes of the molecules in the two adjacent columns. Perfluorobenzobisbenzothiophene 57, in contrast to compound

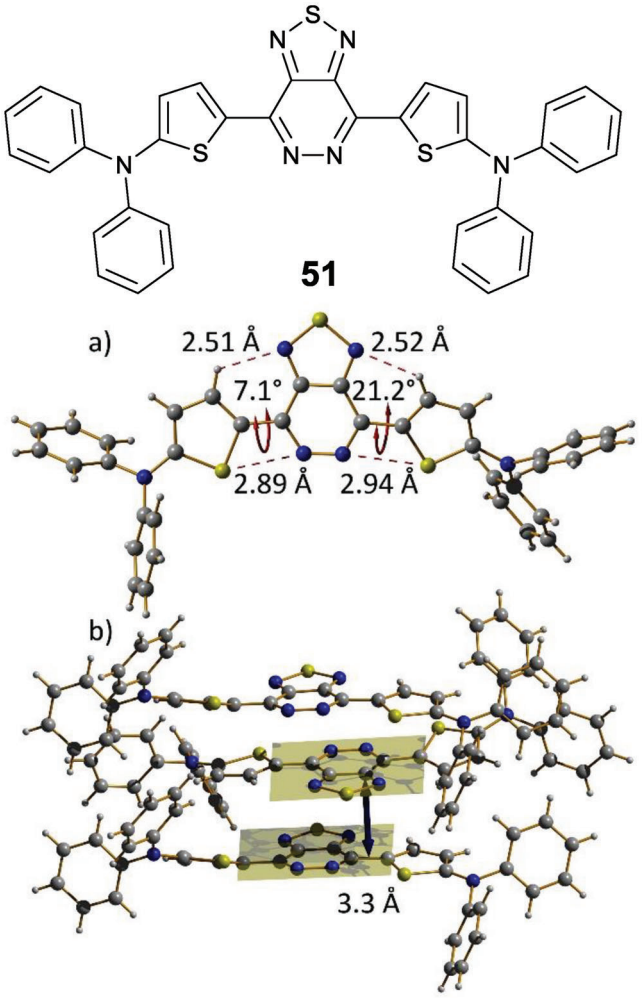

Figure 19. The D-A-D molecular system 51 featuring [1,2,5]thiadiazolo[3,4-d]pyridazine (PT) as an acceptor, its molecular structure a) and antiparallel packing in the crystal b).

56, crystallizes in a triclinic space group P(-1), and the molecules are organized in a staggered manner within the series of parallel planes (Figure 21b) with the distance between planes of 3.33-3.35 Å. Each plane consists of parallel stripes which are stabilized by two sets of S···F close contacts which are shown in Figure 21c by red and blue dashed lines with interaction distances of 3.10 and 3.18-3.19 Å, respectively.

Romito et al. demonstrated another example where altering the structure of fluorinated, chalcogen-containing (Te) organic molecules affects the packing pattern.[55] Fluorinated at the 1-, 3- and 4- positions, [1]benzotelluropheno[3,2:b][1]benzotellurophene 58 was found to crystallize in a herringbone pattern forming a monoclinic crystal with $P2_1/c$ space group. A series of Te···I non-covalent interactions including bifurcated chalcogen bonding (**Figure 22**a) stabilized this type of packing, with a measured distance of 3.65 Å between the stacked molecules in a column, and an angle of 73.4° between the planes of the molecules in the adjacent columns.

When a pyridine unit was introduced instead of a non-fluorinated benzene ring in compound 59, strong halogen···nitrogen interactions were present, in addition to Te short contacts, which led to the formation of a nanoribbon molecular framework (Figure 22b) within the orthorhombic space group Pbca. This supramolecular organization provided closer packing with an inter-plane distance of 3.44 Å (Figure 22c). The close packing of compound 59 resulted in a hole mobility of 8.8×10^{-5} cm^2 V^{-1} s^{-1} in a non-optimized OFET with bottom-gate top-contact configuration, and this compound was used as a hole transport layer in a red-emitting Cu(I)-complex-based light-emitting electrochemical cell (LEC).

3.4. Hydrogen Bonding in Single Molecule Organic Semiconductors

Among the molecular-based organic semiconductors with the classical O···H-N hydrogen bonds the most well-known are organic materials based on the naturally occurring compound indigo. Indigo and its 6,6'-dibromo derivative, Tyrian Purple, were used for dyeing textiles in ancient times. Both these compounds were tried as semiconductors in OFETs and exhibited well-balanced hole and electron mobility values of 0.01 cm^2 V^{-1} s^{-1} for indigo[56] and 0.3 cm^2 V^{-1} s^{-1} for Tyrian Purple.[57] The intramolecular hydrogen bond contributes to a high degree of planarity for the molecule with dihedral angles around the middle bond of only a few degrees. The crystal structures of indigo[58] and Tyrian Purple [59] are very similar, with both compounds forming monoclinic lattices with space group $P2_1/c$. The crystal packing of Tyrian Purple is shown in **Figure 23**a with intra- and intermolecular hydrogen bonds shown by blue and red dashed lines, respectively. The angle between the plane of the molecules in the adjacent columns was found to be 89.6° and the inter-plane stacking distance was 3.4 Å. The effect of molecular structure on the packing in the crystal lattice, which was discussed in the previous section for fluoroorganics, has been observed for indigo derivatives as well. The Mori group investigated the crystal structure and the performance of OFETs containing two indigo derivatives, 60 and 61.[60] The crystal structure of the Tyrian Purple isomer 60 is very similar to that of Tyrian Purple. 5,5'-Dibromoindigo 60 crystallizes within the space group $P2_1/c$ in a herringbone pattern with an angle of 81.01° between the planes of the molecules in the adjacent columns and the same inter-plane stacking distance of 3.4 Å. This packing allowed the maximum hole and electron mobilities of 0.21 and 0.35 cm^2 V^{-1} s^{-1} to be achieved, respectively. Due to the presence of the Br atoms in the molecule, the crystal structure revealed a network of type I halogen bonding interactions[61] (Figure 23b) with close contact distances of 3.61 Å. It is interesting to note that the crystal structure of Tyrian Purple exhibits type II halogen bonding with close contact distances of 3.53 Å (Figure 23c).

Extending the conjugation by two benzene units in compound 61 changes the crystal packing significantly. Although the space group of the crystal remains the same ($P2_1/c$), the herringbone pattern is only seen at the positions of phenyl rings which form a dihedral angle of 28.3° with the planar core unit. The latter is only tilted by 14.5° in molecules related to each other by a screw axis symmetry, so efficient charge hopping is possible between them and high hole and electron mobilities of 0.56 and 0.95 cm^2 V^{-1} s^{-1}, respectively, were measured. The intra- and

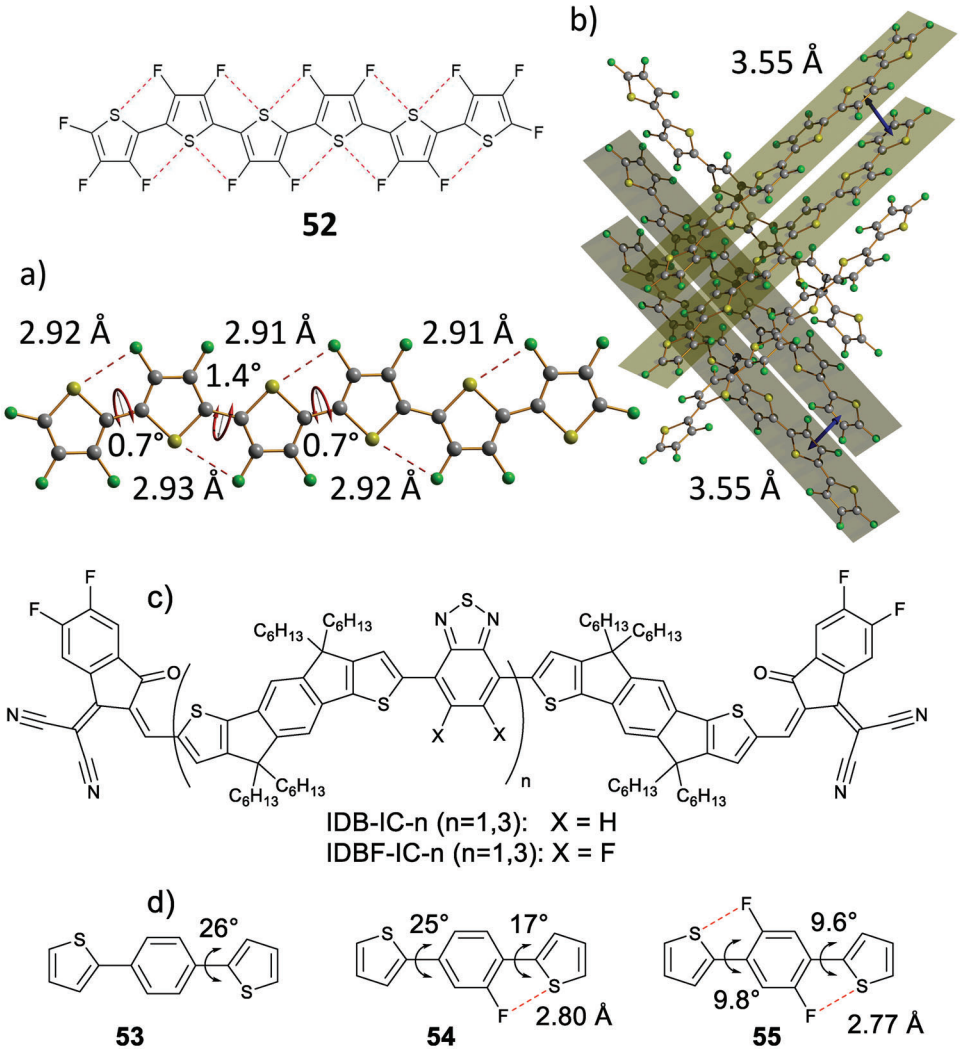

Figure 20. The molecular structure of tetradecafluorosexithiophene a), molecular packing into columns oriented by 84.7° to each other b), NFAs featuring the advantage of S···F conformational lock c) and the compounds 53–55 used for the measurements of the single molecule conductance (the dihedral angles and S···F distances estimated by DFT geometry optimisation).

intermolecular interactions between the molecules located in the plane (0,1,0) stabilize this packing (Figure 23e)

In Section 3.1, two n-type organic semiconductor materials 35 and 36 (Figure 10) with a central ThDPP core and terminal DCIM units were highlighted with both S···O non-covalent interactions and O···H hydrogen bonding present. These materials showed maximum electron mobilities of 0.18 and 0.77 $cm^2\ V^{-1}\ s^{-1}$, respectively.[31] The ThDPP core unit was also featured in a series of p-type organic semiconductors, the structures of which were resolved by single crystal X-ray analysis. The structures varied with the core decorated with pyrene 62[62] and arms containing heteroatom-substituted indene structures 63–65 (**Figure 24**).[63] The crystal structure of compound 62 revealed π-π stacking interactions between pyrene donor groups with an inter-plane distance of 3.5 nm. These stacking interactions are beneficial for efficient hole transport and BHJSCs fabricated using compound 62 as a donor and $PC_{71}BM$ as acceptor showed a maximum PCE of 4.1%.

The effect of heteroatom substitution has been investigated by studying the crystal structures of the ThDPP central unit end-capped with benzofuran (63a), benzothiophene (63b) and N-methylindole (63c).[63a] The more efficient packing of the molecule 63a was found to be due to the smaller size of the oxygen atom of the benzofuran unit. The π-π interactions of molecule 63b were hindered by sulfur-sulfur repulsion. The least efficient molecular packing was found in compound 63c due to the twisted conformation of the molecule. The measured maximum OFET mobility values were found to follow the trend of the efficiency of the packing interactions and decreased in the series 63a ($5.3 \times 10^{-4}\ cm^2\ V^{-1}\ s^{-1}$) > 63b ($4.3 \times 10^{-5}\ cm^2\ V^{-1}\ s^{-1}$) > 63c ($1.5 \times 10^{-5}\ cm^2\ V^{-1}\ s^{-1}$).[63a] The OFET hole mobility of 63a was increased to $2.8 \times 10^{-4}\ cm^2\ V^{-1}\ s^{-1}$ after using chiral alkyl chains in the meso-isomer of 63a, due to improved π-π stacking interactions.[63b] Compound 63a showed best performance in BHJSCs compared to 63b and 63c when used in a blend with $PC_{71}BM$, exhibiting a PCE of 4.8%.[63a]

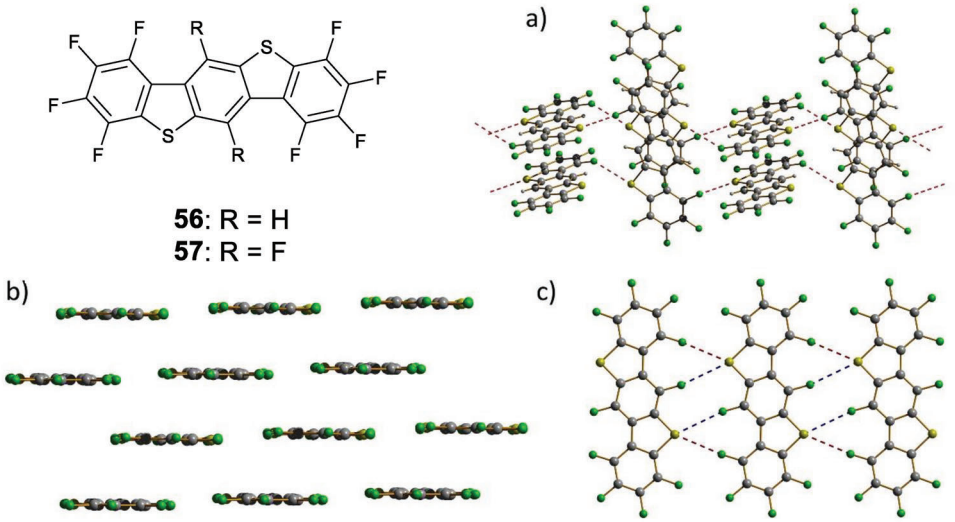

Figure 21. The herringbone packing of compound 56 and the infinite planes of compound 57 in the crystals assisted by S···F non-covalent interactions.

Another example of ≐O···H–C hydrogen bonding can be seen in the structure of 3,7-bis((E)-5,7-difluoro-1-(2-ethylhexyl)-2-oxoindolin-3-ylidene)-3,7-dihydrobenzo[1,2-b:4,5-b']difuran-2,6-dion (F_4-BDOPV).[64] The crystal structure of F_4-BDOPV revealed a centrosymmetric distorted molecule with extremely short C≐O···H–C hydrogen bonds of 2.07 Å (red dashed line) and 2.08 Å (blue dashed line) (Figure 24). The low lying LUMO level of −4.44 eV provides greater ambient stability of this *n*-type material. Due to co-facial packing, the material exhibits a high electron mobility of 12.6 $cm^2\ V^{-1}\ s^{-1}$ in a single crystal OFET.

As mentioned before in Section 3.1, non-covalent interactions have been successfully applied for the design of non-fused NFAs. S···O and S···F conformational locks have been established in the crystal structures of FOC2C6-2FIC and FOC6-IC (Figure 14).[41] However, the simplest structures of non-fused NFAs are those that feature the >O···H–C hydrogen bonding motif and based on the PTIC structure (PTIC,[65] PTB4F, and PTB4Cl[66] (Figure 24)). The single crystal X-ray diffraction studies of PTIB4F, PTB4Cl,[66] and PTIC[67] reveal that the lengths of the hydrogen bonds are 2.24, 2.23, and 2.23 Å, respectively. The crystal structure of PTIB4F exhibited mixed model stacking and showed a wider lamellar arrangement which would undermine the charge and exciton transport. PTB4Cl molecules are arranged in A-to-A and A-to-D type stacking with a π-π stacking distance of 3.5 Å and the intermolecular distance between two chlorine atoms was 3.33 Å.[66] PTIC molecules adapt a

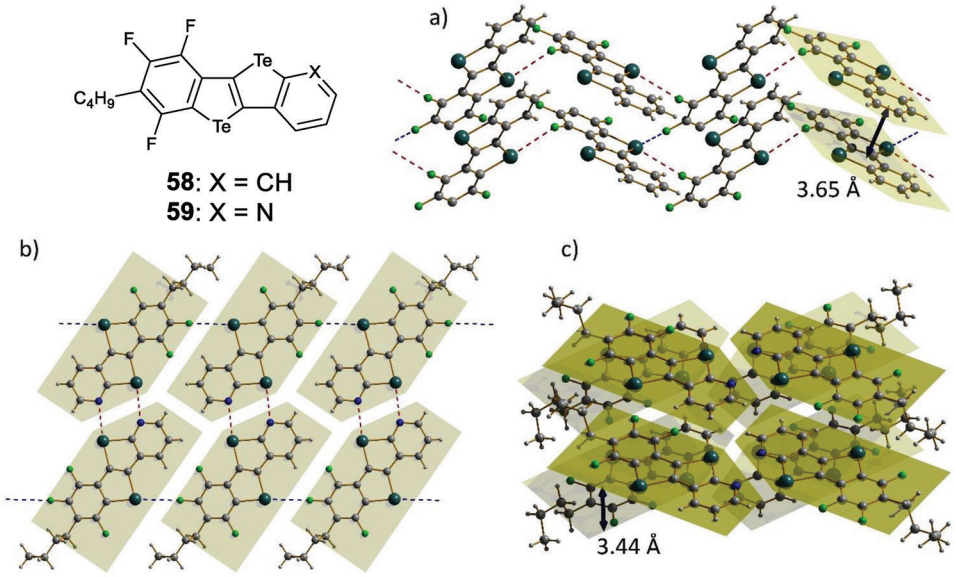

Figure 22. The telluropheno[3,2:b]tellurophene based fluorinated compounds (58-59), the herringbone packing of compound 58, with the two set of Te···F short contacts shown by red (3.26 Å) and blue dashed lines (3.49 Å) a), supramolecular nanoribbon formed by compound 59 b) and its packing c).

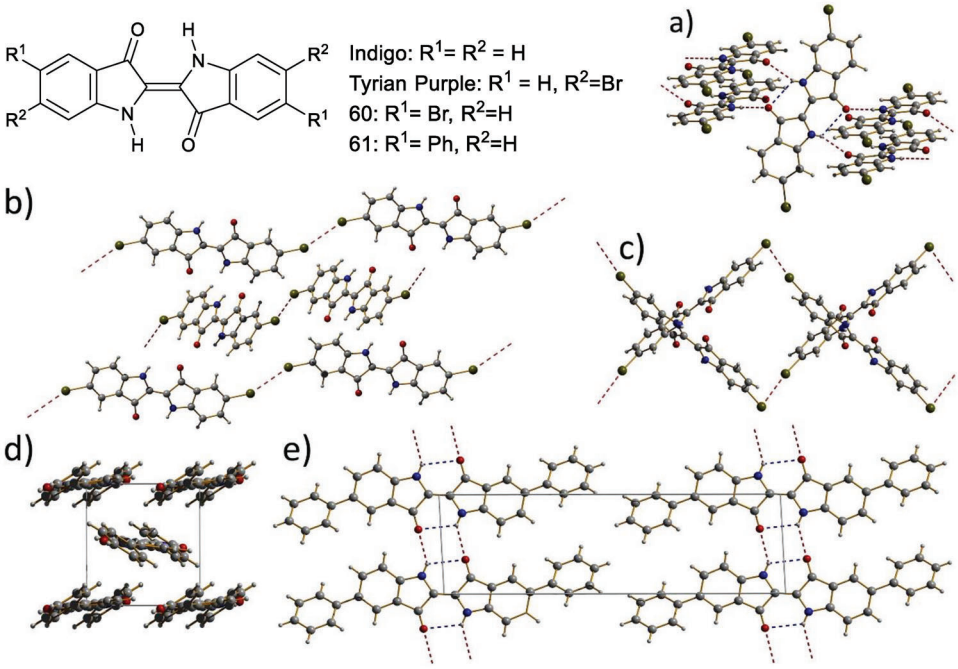

Figure 23. The structure of indigo based semiconductors with classic ≐O···H–N< hydrogen bonding. The hydrogen bonded network in the crystal packing of Tyrian Purple a), the halogen bonding interactions in the crystal of compound 60 b) and Tyrian Purple c), the view along the *a* axis in the unit cell of the crystal of 61, the intra- and intermolecular hydrogen bonds between the molecules located on the (0,1,0) plane of the unit cell.

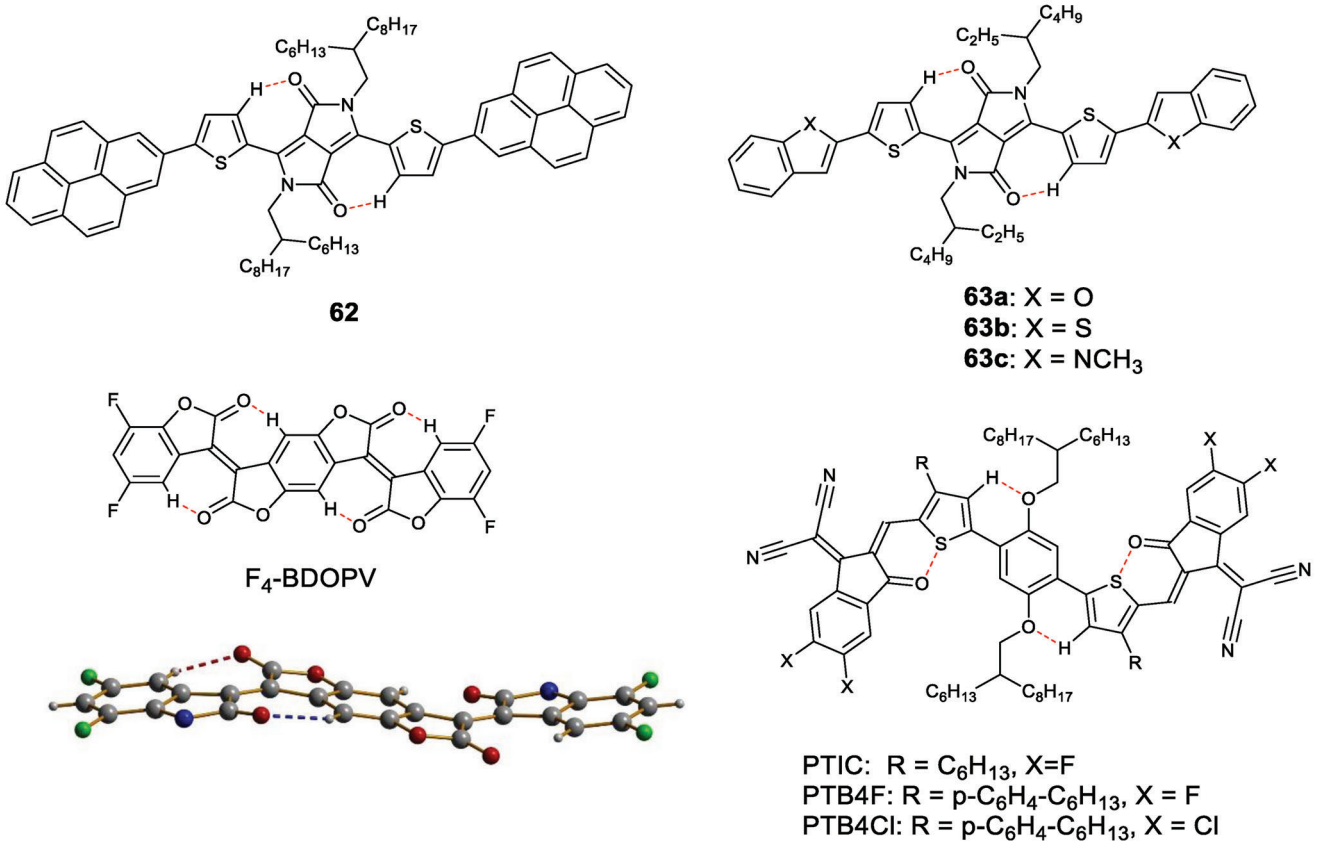

Figure 24. The structure of organic semiconductors featured with O···H–C type of hydrogen bonding.

"brick-like" end-to-end stacking with inter-plane distance of 3.37 Å.[67] The SCLC hole/electron mobility for PTB4Cl, PTB4F, and PTIC was found to be 7.65×10^{-5} cm^2 V^{-1} s^{-1}/8.62×10^{-5} cm^2 V^{-1} s^{-1}, 3.53×10^{-6} cm^2 V^{-1} s^{-1}/7.82×10^{-6} cm^2 V^{-1} s^{-1}, and 5.57×10^{-5} cm^2 V^{-1} s^{-1}/8.23×10^{-5} cm^2 V^{-1} s^{-1}, respectively.[66]

Among the three NFAs (PTIC, PTB4F, and PTB4Cl), PTB4Cl exhibited the highest performance of its blend with PBDB-TF in a BHJSC, achieving a PCE of 12.76%, which is the highest value reported so far for a non-fused NFA.[66] The PCE of the BHJSC fabricated from the blend of ITIC with PBDB-TF was found to be as high as 10.28% and this non-fused NFA exhibited exceptional photostability compared to the other fused (IT-4F) and semi-fused (HF-PCIC) A-D-A NFAs due to the presence of a hexyl chain on the thiophene ring.[67] The high performance, simple synthesis and exceptional photo-stability make PTIC-based NFAs a good model system for developing cheap, efficient, and stable OPVs.

4. Heteroatom Interactions in Polymers

It was "for the discovery and development of conductive polymers" that Heeger, MacDiarmid and Shirakawa were awarded the Nobel prize for Chemistry in 2000 and thus, polymers have been key to the advancement of "synthetic metal"/organic semiconductor materials. While hydrocarbon-based polymer polyacetylene was a large part of the groundwork in this field, introducing heteroatoms into polymer structures quickly contributed to the advances achieved in these types of materials as a means to overcome the challenging processing conditions and poor stability of polyacetylene.

One of the most well-known heterocyclic polymers is poly(3-hexylthiophene) (P3HT) which has been used as a donor in BHJSCs,[68] a *p*-type material in OFETs[69] and in sensing devices,[70] for example. Early research on this polymer was motivated to improve the regioregularity of the polymer, ensuring a head-to-tail conformation, as regiorandom P3HT was shown to have a higher band gap due to more twisting in the polymer chain as a result of head-to-head linkages.[71] It was the synthesis conditions that were optimized to improve the regioregularity of P3HT by using a Grignard reagent[72] or using an organozinc monomer.[73] However, it was soon discovered that heteroatoms in the polymer side chain could help influence the conformation in the same way, whilst being less sensitive to the reaction conditions, leading to a more diverse range of materials that could be created in a favorable conformation.

As polymer structures have become more complex in the pursuit of desirable organic semiconductor device properties, it has also become more difficult to determine the true influence of non-covalent interactions by simply analyzing physical properties, such as the band gap. As detailed in Section 3, the most common means to determine the influence of non-covalent interactions in small molecules is to examine structures generated from single crystal X-ray diffraction studies. Theoretical calculations (commonly DFT) are also often used to determine which conformation is most energetically stable. When analyzing the effect of heteroatom interactions in polymers, single crystal X-ray crystallography cannot be used. Therefore, the crystal structures of the constituent monomers can be used to infer the most stable conformations along the polymer backbone. Similarly, while models of the effective conjugation length for polymers can be used in theoretical calculations of polymers,[74] the computational cost of model oligomers is large. Therefore, energy calculations for conformers of different monomers are normally used as a means of determining the influence of heteroatom interactions.

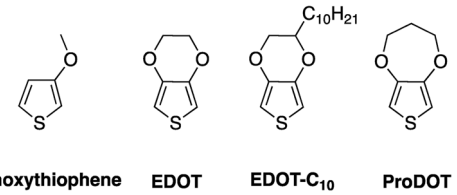

Figure 25. Monomers used for the synthesis of poly(alkylenedioxythiophene) materials reported by Heywang and Jonas.[76]

In the following section, we detail examples of common heteroatom-heteroatom interactions and the analyses that determined the influence of these short contacts. We highlight how the use of sulfur-oxygen interactions in the pursuit of improved polythiophenes has inspired a synthetic tool for improved polymer performance, and one that is still evolving. We also highlight how the interaction of sulfur and other heteroatoms, nitrogen and fluorine, as well as the use of hydrogen bonds can be used for improved polymer performance.

4.1. S···O Interactions in Polymers

As highlighted in the previous section, sulfur-oxygen interactions are prominent in the choice of non-covalent interactions to planarise molecular structures, and this is also true for polymers. The first example of thiophene monomers that could be used to create polymers with sulfur-oxygen interactions was demonstrated in a patent by Bayer AG,[75] some of which was reported in 1992 by Heywang and Jonas (**Figure 25**).[76] The motivation for this work was to stabilize the positively charged, doped polymer, in pursuit of higher and more stable conductivity. From the monomers tested, 3,4-ethylenedioxythiophene (EDOT), 2-decyl-2,3-dihydrothieno[3,4-b][1,4]dioxin (EDOT-C_{10}) and 3,4-propylenedioxythiophene (ProDOT) all exhibited conductivity greater than 1 S cm^{-1}, an increase of 3 orders magnitude when compared with polypyrrole, and EDOT showed improved thermal stability in the polymerization reaction, with the oxidative polymerization reaction being carried out in boiling benzonitrile giving PEDOT with a further enhanced conductivity of up to 31 S cm^{-1}.[76] Moreover, the stability of PEDOT was demonstrated with a PEDOT-coated polycarbonate film when it showed very little change in resistivity when exposed to H_2O vapour at 100 °C for 25 h. This was in stark contrast to polypyrrole films where the surface resistance increased by four orders of magnitude over the same time period.[76]

Therefore, the use of alkylenedioxythiophenes, EDOT in particular, was successful as a means of improving conductivity and imparting good stability on polythiophene-based materials. However, the idea of sulfur-oxygen interactions in EDOT-based materials wasn't explicitly suggested until 2000 in a study of EDOT-containing oligomers by Turbiez and co-workers.[77] Now, it is one

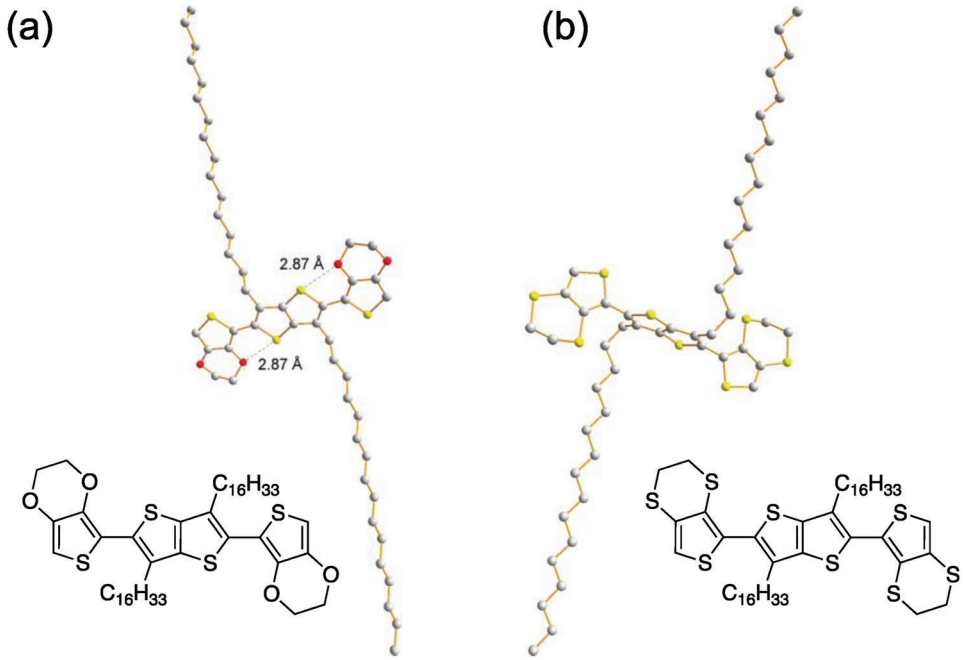

Figure 26. Crystal structures of a) EDOT-containing and b) EDTT-containing bithiophene monomers reported by McEntee and co-workers. Reproduced with permission.[78] Copyright 2010 American Chemical Society.

of the most commonly observed planarizing interactions in polymer materials for a range of applications from high conductivity materials to donor materials for solar cells.

The extent of which the planarizing of the polymer backbone can affect the physical properties of the polymer can be observed when comparing the polymers made by electrodeposition of EDOT and ethylenedithiathiophene (EDTT) based monomers (**Figure 26**), reported by McEntee and co-workers.[78] The monomers show a clear structural difference, with the sulfur-oxygen interactions causing planarization of the unit while the EDTT-containing molecule is twisted due to repulsive sulfur-sulfur interactions. This causes a reduction in the HOMO-LUMO gap, measured by cyclic voltammetry, 0.24 eV.[78] However, the effect is more pronounced when the monomers are electropolymerized, with the resulting EDOT-containing polymer showing a band gap (E_g = 1.53 eV), measured using solid-state cyclic voltammetry, that is almost 1 eV lower than EDTT-based polymer (E_g = 2.49 eV).[78] This is caused by lengthening of the conjugation length in the planar polymer and highlights that the choice of non-covalent interaction can cause substantial differences in polymer properties.

Guo and co-workers reported a series of phthalimide-bithiophene-based polymers (**Figure 27**) with structures designed to observe the influence of these interactions.[79] The bithiophene groups can be divided into three groups: i) bisalkylated (P1) and dithienopyran (P3), which would not have any sulfur-oxygen interactions present in the bithiophene repeat unit, ii) 3-alkyl-3′-alkoxy-2,2′-bithiophene (P5a-c) and 3-alkoxy-2,2'-bithiophene (P4), where one intramolecular sulfur-oxygen interaction is present in the bithiophene unit, and iii) 3,3'-alkoxy-2,2'-bithiophene (P2) where two non-covalent interactions exist. The result is that P2 shows a significantly higher hole mobility ($1.45\ cm^2\ V^{-1}\ s^{-1}$) than the other polymers while polymers P5a-c show a moderate-to-high hole mobility, depending on the choice of side chain.[79] Interestingly, the lack of alkyl side chain in P4 contributes to no p-type mobility being observed in OFET devices due to poor film-forming properties.[79] However, despite having the highest hole mobility, P2 doesn't perform as well as a donor material as polymers P5a-c in BHJSC devices.[79] This can be explained by the reduction in open-circuit voltage caused by the increase in electron density as a result of using two alkoxy side groups. Therefore, it is important to be mindful of this effect when incorporating electron-rich alkoxy side groups into donor materials for OPVs.

One of the most exciting and timely areas of research that has broadened the concept and application of synthetic metal-inspired materials is the use of organic mixed ionic and electronic conductor (OMIEC) polymers for organic electrochemical transistors (OECTs). It is also one area where sulfur-oxygen interactions have been used with profound success. In polymers for such devices, it is critical to enhance both electrical and ionic conduction and poly(thiophenes) functionalized with oligoether side chains fulfill both of these requirements with a planar, rigid polymer backbone and hydrophilic side groups. These materials are inspired by PEDOT:PSS, which has a rigid poly(ethylenedioxythiophene) backbone, but aim to overcome problems such as the presence of insulating poly(styrene sulfonate) and the need to operate the OECT in depletion mode.

The first example of a neutral polymer used in aqueous, bulk-gated OECTs was demonstrated by Giovannitti and co-workers, who compared poly(2-(3,3′-bis(tetradecyloxy)-[2,2″-bithiophen]-5-yl)thieno[3,2-b]thiophene (p(a2T-TT)) and poly(2-(3,3′-bis(2-(2-(2-methoxyethoxy)ethoxy)ethoxy)-[2,2″-bithiophen]-5-yl)thieno[3,2-b]thiophene) (p(g2T-TT)) and

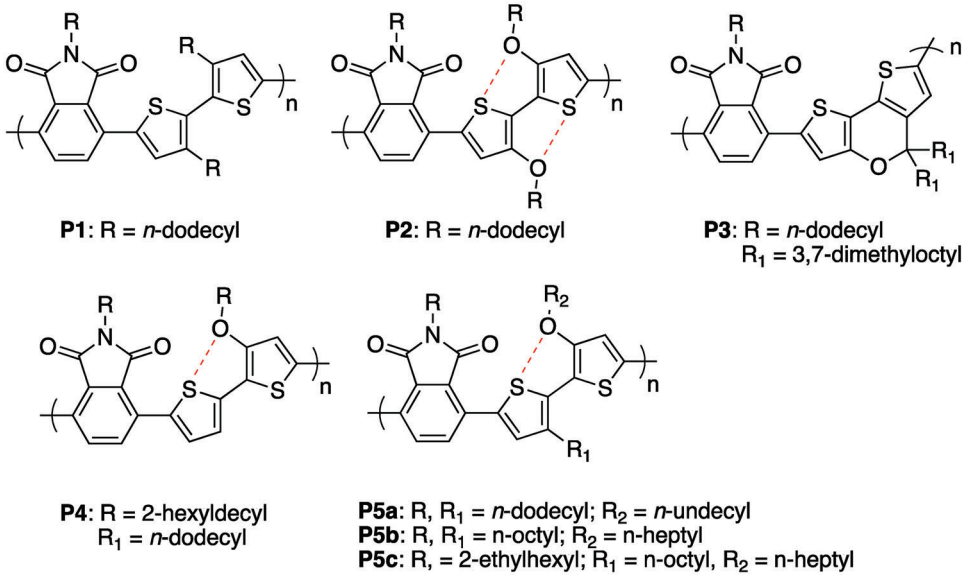

Figure 27. Structures designed for the investigation of sulfur-oxygen interactions in phthalimide-bithiophene-based co-polymers by Guo and co-workers.[79]

highlighted the improvements in switching and high transconductance achieved with the polymer containing glycolated side chains.[80] The structures of these polymers are shown in **Figure 28**. Although this work doesn't specifically highlight the importance of sulfur-oxygen intramolecular interactions, as both polymers have the same interactions occurring, the justification of choosing such a rigid polymer backbone with expected high mobility is made.[80] This has inspired further improvements of OECTs with polythiophene-oligoether-based materials[81] and it is evident that the charge transporting properties achieved with the use of sulfur-oxygen interactions has played a significant role in the success of these materials.

Using sulfur-oxygen interactions induced from the oxygen of ether groups bound to carbon atoms in the 3- or 4- position of thiophene derivatives is a common way to improve the planarity of polymers. However, in the examples above, the introduction of alkoxyl groups in the thiophene monomer causes the resulting polymer to have a significantly increased HOMO energy, while the LUMO can be similarly affected, albeit to a lesser extent in the case of donor-acceptor polymers. This can be especially detrimental for donor materials in OPV active layers as an increased HOMO energy can result in a reduced open-circuit voltage, reducing the PCE that can be achieved.[82] Huang and co-workers introduced a novel way to mitigate against this, yet still utilise sulfur-oxygen interactions as a conformational lock.[28] This involved using a modified thienyl-vinyl-thienyl (TVT) group with alkoxy groups attached to the alkene unit. This functionality was also used in conductance studies of di(thiophen-2-yl)benzene-based single molecules, described in Section 3.1. Through single crystal X-ray diffraction, the authors showed the monomer (**Figure 29**a) to have an intramolecular S···O distance of 2.690 Å, suggesting that it is a fairly strong interaction, and the structure is planar.[28] Alkyl side groups used in place of the ethoxy side chain cause the thiophenes to twist, highlighting the advantage of using the non-covalent interactions. The alkoxy-bearing monomer could be used to make distinctly *n*-type and *p*-type thin film transistors using an NDI (P8, Figure 29c) or benzodithiophene (P9, Figure 29c) co-monomer, resulting in high electron and hole mobilities, in air, of 0.5 $cm^2\ V^{-1}\ s^{-1}$ and 0.05 $cm^2\ V^{-1}\ s^{-1}$, respectively.[28]

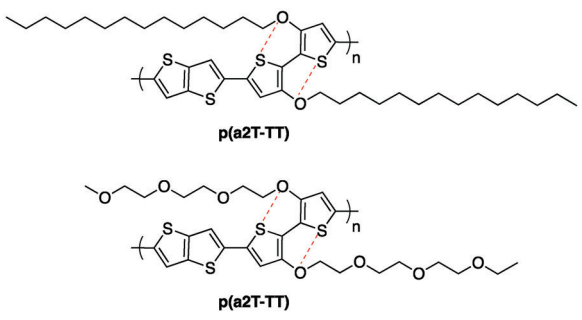

Figure 28. Structures of polymers reported by Giovannitti and co-workers for aqueous, bulk-gated OECTs.[80]

Further diversity in polymer structures where these intramolecular interactions can be observed was demonstrated in a recent work by Sinclair and co-workers, who present the use of *N*-oxidation of bisthiazole systems.[83] Molecular and polymer structures were created with this approach (**Figure 30**) and it is observed that the formation of one *N*-oxide results in a narrowing of the band gaps, which are further reduced when two *N*-oxide groups are introduced to the bisthiazole unit.[83] This supports the predicted rigidification as a result of the sulfur-oxygen interactions induced by the oxidation. The simplicity of the oxidation steps of the bisthiazole unit is a benefit compared to the synthetic steps required to introduce ether groups in thiophene derivatives–it represents an easy way to introduce sulfur-oxygen interactions into a polymer backbone. For this reason, we may see more examples of polymers with *N*-oxidized

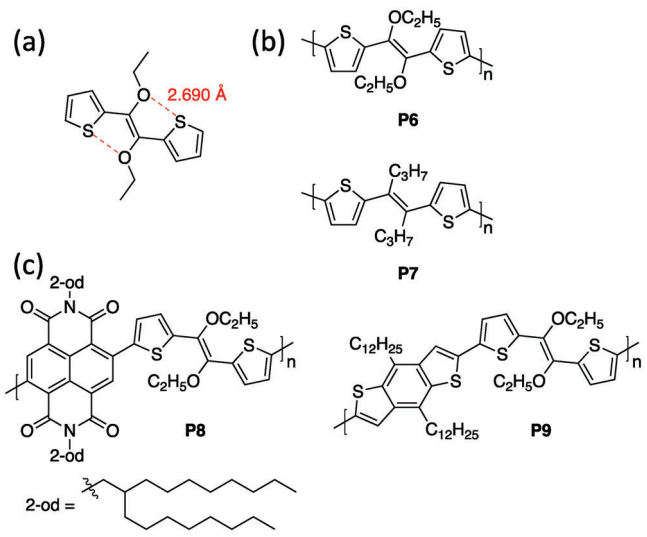

Figure 29. a) Sulfur-oxygen interaction of alkoxyl-modified TVT monomer with the intramolecular distance measured from X-ray crystallography highlighted; b) polymer P6, containing alkoxyl-modified vinylene group and alkyl analogue P7; c) structures of polymers P8 and P9 used in OFET devices. Reported by Huang and co-workers.[28]

bisthiazole reported for organic semiconductor applications in the future.

Another alternative to ether functionalities are ester groups which have also been successfully used to induce sulfur-oxygen interactions. Chen et al. designed a polymer to improve on existing sulfur-oxygen interactions from an alkoxy side group and thiophene unit by introducing ester side chains on adjacent thiophenes (**Figure 31**a).[84] The effect of the sulfur-oxygen interaction through the carbonyl of the ester is most evident when analyzing the crystal structures of the monomers. The sulfur-oxygen distance of the ether oxygen and its adjacent sulfur (2.66 Å) is reduced by 0.24 Å compared to the analogous interaction in the polymer with only ether oxygen atoms (Figure 31b).[84] The sulfur-carbonyl oxygen distance is 2.63 Å, showing that the addition of the ester side chain rigidifies and compacts the monomer.[84] This leads to improved aggregation in the resulting polymer which causes a marked increase in the PCE of OPV devices. Not only did the ester groups improve the backbone planarity of the polymer but its electron withdrawing nature counteracts the rise in HOMO energy cause by using ether groups, leading to improved open circuit voltage in the resulting OPV devices.[84] This can therefore be considered an especially effective strategy to planarize polymers to be used as donor materials for OPV devices.

Similarly, ketone functionalities in electron-deficient acceptor materials can be valuable in controlling the conformation of polymer backbones. A study by Guo and co-workers in 2012 compared polymers containing bithiopheneimide (BTI) and thieno[3,4-c]pyrrole-4,6-dione (TPD) acceptor units, where the proximity of the sulfur of the neighbouring dithienosilole unit to the acceptor's ketone groups varies, with TPD being closer.[85] The TPD-containing polymer, PTDPSi-C8, had a slightly reduced band gap compared to the BTI-based polymer, PBTISi-C8.[85] However, there is also a striking difference in the absorption profile of the polymers (**Figure 32**a), with the spectra of PTDPSi-C8 showing more fine structure in both solution and thin film.[85] This suggests that there is improved aggregation in PTPDSi-C8. DFT calculations of the respective monomers showed a twist in PBTSi of 11°, whereas the PTPDSi monomer was planar (Figure 32b).[85] The improved planarity is induced by the sulfur-oxygen interactions, and this in turn causes improved aggregation of the polymer chains. As a result, OPVs using PTPDSi-C8 as a donor material show a highest performance of 6.83% efficiency, when comparing the two polymers, caused by an improved fill factor and open-circuit voltage. Grazing-incidence wide-angle X-ray scattering (GIWAXS) was used to better understand the OPV device characteristics, with PTPDSi-C8 shown to have closer interchain stacking distances (20.1 Å) compared to PBTISi-C8 (21.8 Å).[85] This again highlights how conformational control of a polymer chain is important for improving bulk properties of semiconductor materials.

Given, the versatility of different oxygen-containing functionalities, it is important to determine which sulfur-oxygen interactions may be most influential. Thorley and McCulloch carried out a theoretical study, using natural bond orbital analysis to study charge-charge, dipole-dipole and charge-dipole interactions for sulfur-oxygen and sulfur-fluorine contacts.[86] From this perspective, it is important to get a balance between strong charge-dipole interactions and avoiding dipole-dipole repulsion. As a result, carbonyl groups generally are more effective than alkoxy functionalities due to an increased dipole moment.[86] However, a general design rule from this study was that oxygen (or fluorine) dipoles should be positioned directly in the direction of the sulfur atom to strengthen the non-covalent interaction.[86] Therefore, the angle at which an interacting atom sits with respect to its counterpart is of importance.

Overall, it has been shown how the desire to improve the conductivity in synthetic metal polymers has led to the discovery of a design tool to help improve the planarity of polymers chains. Furthermore, synthetic chemists have been able to develop ways to increase the diversity in the functionalities capable of having such an influence. This increased the control of resulting physical properties for polymers. As a consequence, sulfur-oxygen interactions have been, and will continue to be, used in materials which advance the performance of semiconductor devices such as OFETs, OPVs, and OECTs.

4.2. Sulfur-Nitrogen Interactions in Polymers

Similar to the interaction between sulfur and oxygen, sulfur-nitrogen non-covalent interactions result from electrostatic interaction from the lone pair of electrons in nitrogen atoms toward sulfur atoms with a partial positive charge.[14] Therefore, as highlighted in the small molecules section, nitrogen-containing heterocycles are a useful building block to support non-covalent short contacts which enhance planarity and these types of structures have been used in polymers as a means to create polymers with a planar backbone.

Thiazole is a particularly popular heterocycle used to introduce sulfur-nitrogen interactions in polymers. For example, in 2013 Bronstein and co-workers introduced new isostructural analogues to P3HT, PTTz, and PTTTz (**Figure 33**a). These

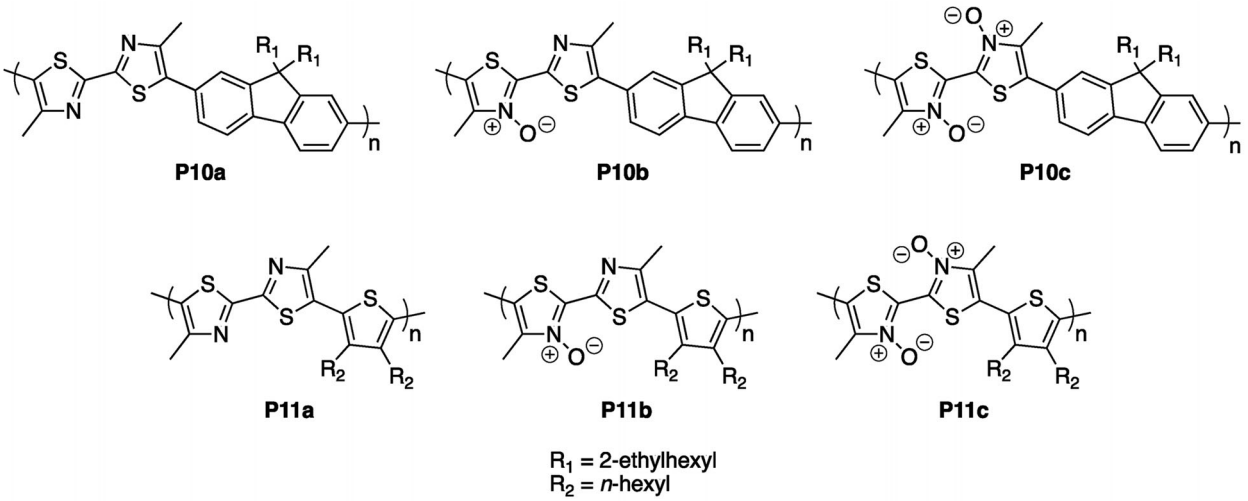

Figure 30. Polymers formed with N-oxidised bisthiazole co-monomers.[83]

polymers contain hexylthiazole units in the polymer backbone and it was shown from a potential energy scan (Hartree-Fock/Aug-cc-pVDZ, MP2 peturbative corrections) that there is substantial stabilization in the head-to-tail conformation when thiazole is introduced, compared with the thiophene dimer (Figure 33b). The authors showed that the reason for this is due to donation of the lone pair of the nitrogen on the thiazole to the antibonding orbital of the thiophene's sulfur atom.[87]

Whilst PTTz and PTTTz are *p*-type semiconductors, the sulfur-nitrogen interactions of 2,2'-bithiazole results in a planar, electron-withdrawing unit which has been used successfully in n-type polymer materials for OFETs. For example, it had been used in co-polymers with dithienyldiketopyrrolopyrrole and dipyridynyldiketopyrrolopyrrole co-monomers, resulting in solely n-type behavior and mobilities of 0.3 $cm^2\ V^{-1}\ s^{-1}$[88] and 0.05 $cm^2\ V^{-1}\ s^{-1}$,[89] respectively. The application of thiazole groups in p-type and n-type polymers highlights the versatility of this building block, with the electron-deficient nitrogen being useful to reduce the ionization energy (relative to vacuum) of hole transporting polymers or decrease the LUMO and improve charge transport in electron transporting materials.

Liu et al. carried out an in-depth theoretical study to uncover the effects of non-covalent interactions on the electronic properties of polymers, other than conformational control.[90] The

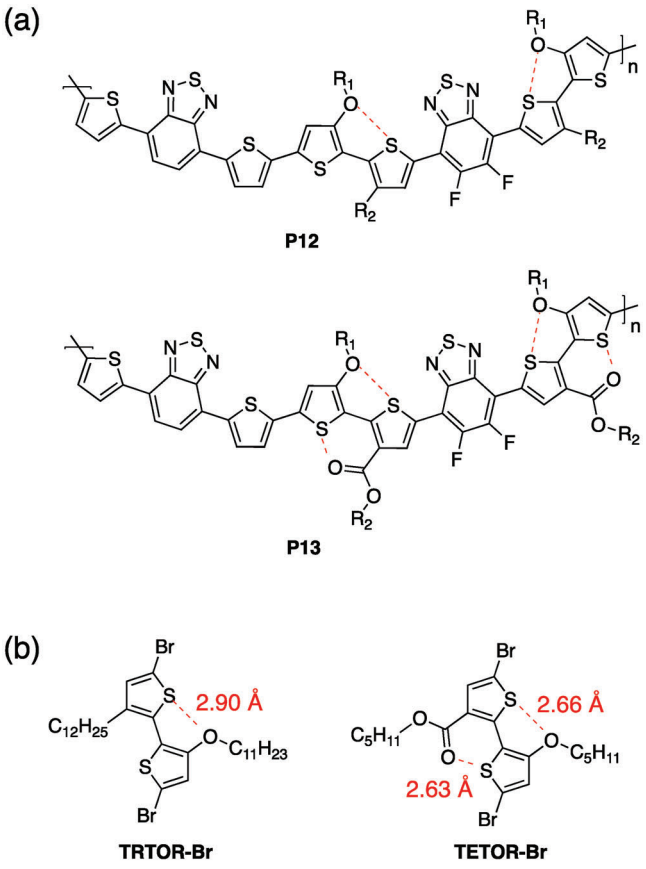

Figure 31. a) Structures of polymers reported by Chen and co-workers with sulfur-oxygen interaction induced using ether, and ether and ester groups; b) intermolecular distances measured from single crystals of monomer units.[84]

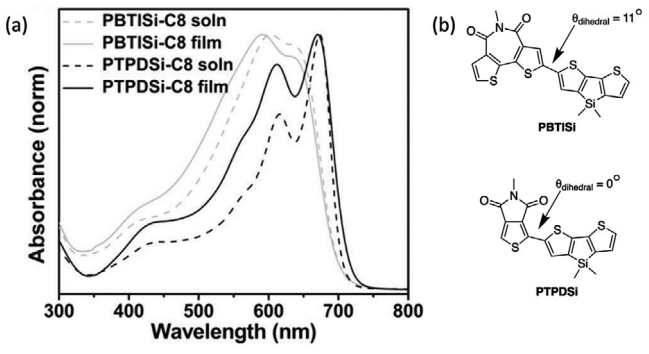

Figure 32. a) Absorption profile of polymers PTBTISi-C8 and PTPDSi-C8 in solution (dashed line) and thin film (solid line) and b) depiction of the dihedral angles of monomers for PBTISi and PTPDSi reported by Guo and co-workers. Reproduced with permission.[85] Copyright 2012, American Chemical Society.

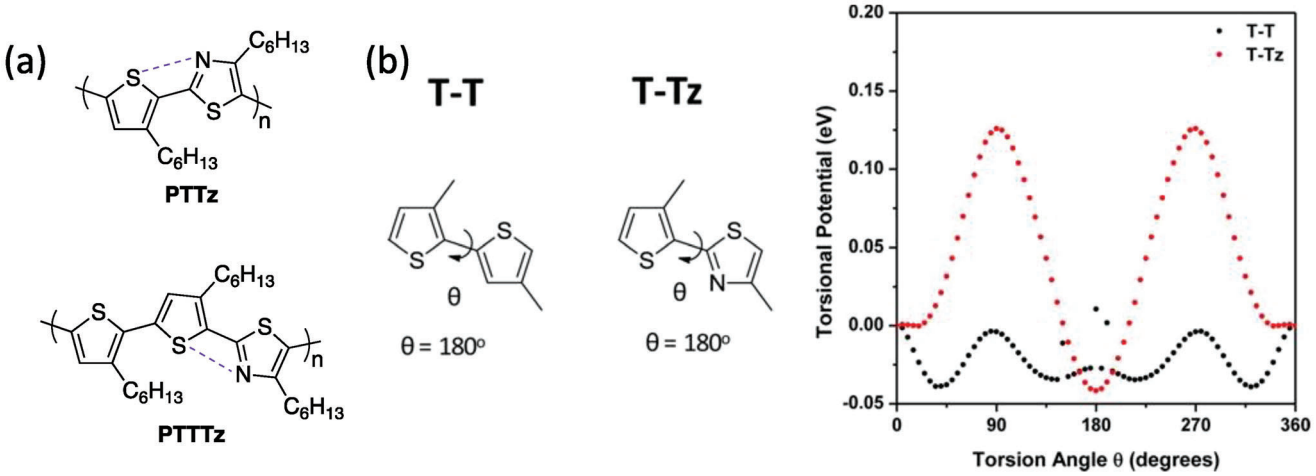

Figure 33. a) Structures of hexyl-thiazole-containing polymers PTTz and PTTTz reported by Bronstein and co-workers and b) potential energy dihedral scan of methylthiophene-dimer and methylthiophene-methylthiazole unit. Reproduced with permission.[87] Copyright 2013, American Chemical Society.

band gaps of polymers containing different non-covalent interactions (sulfur-nitrogen, sulfur-oxygen, sulfur-fluorine, oxygen-nitrogen, oxygen-fluorine, and nitrogen-fluorine) with different conformers, where the torsional angle between the interacting groups was rotated 180°, were compared. Sulfur-nitrogen interactions were especially effective in reducing the band gap, with conformers showing a band gap up to 0.15 eV lower than the C–H···N interacting conformer. This originated from an increase in the HOMO energy (relative to vacuum) while the LUMO is largely unaffected. Using an adiabatic rate equation, the authors determined that the hole hopping rate was increased when sulfur-nitrogen interactions were present in the polymer conformation. It was proposed that there was effective charge redistribution as a result of the heteroatom interaction, which causes stabilization of the quinoid structure of the polymer. From this perspective, the sulfur-nitrogen interactions were more effective than the other non-covalent interactions studied. However, it should be highlighted that all of the models containing sulfur-nitrogen interactions that were studied were based on benzothiadiazole and similar analogues, meaning that this analysis may not hold for other types of sulfur-nitrogen interaction.

As a tool for design of semiconducting polymers, it can be considered that certain kinds of sulfur-nitrogen interactions, as detailed by Liu et al. have considerable influence on the polymer's bulk properties. However, in general, sulfur-nitrogen interactions are not as widespread or unambiguous as sulfur-oxygen interactions. Nonetheless, sulfur-nitrogen non-covalent contacts can be used effectively in n-type and ambipolar materials, where the use of sulfur-oxygen interactions are not possible if using electron-rich alkoxythiophene groups, for example.

4.3. Sulfur-Fluorine Interactions in Polymers

There has been much recent work on introducing fluorine atoms into polymers in order to improve organic semiconductor device performance. This is likely inspired by the evolution of both donor and acceptor materials for OPVs, where introducing fluorine atoms has helped achieve high power conversion efficiencies. Prominent examples of polymers which feature sulfur-fluorine are OPV donor materials PTB7-Th (also known as PCE10 and PBDTTT-EDT),[91] PffBT4T-2OD (also known as PCE11)[92] and PM6 (also known as PBDB-T-2F or PBDB-TF).[93] PM6, in particular, has been used in benchmark OPV devices, achieving 15.7%[37] PCE in a bulk heterojunction device with the non-fullerene acceptor Y6 and 19.6% PCE in a tandem device containing active layers of PM6:ITCC and PM6:BTP-eC11.[94] Often the improved performance of donor polymers functionalized with fluorine atoms is attributed to the reduction (relative to vacuum) in the ionization energy, which can improve the open-circuit voltage.[95] However, there are cases where the short-circuit current or charge mobility improves and can be attributed to improved crystallization of the polymer or more optimum phase separation in the donor-acceptor blend.[92,93] Therefore, it is important to assess whether non-covalent interactions between sulfur and fluorine play a role in improving the material's performance.

In 2013, Bronstein and et al. reported indacenodithiophene-based donor-acceptor polymers where the acceptors used were 2,1,3-benzothiadiazole and 5,6-difluoro-2,1,3-benzothiadiazole (**Figure 34**).[96] The optical properties of the two polymers are very similar but slight red-shifted absorbance maximum and onset in the thin film spectrum, as well as the appearance of a shoulder at shorter wavelength, suggests that the fluorinated polymer is more rigid and undergoes better packing in the thin film.[96] Theoretical calculations of representative monomers showed that the potential energy surface was steepened close to the minimum energy structure for the fluorinated compounds and this should result in improved planarity in polymers.[87] The hole mobility of P15 ($\mu_{saturated}$ = 0.065 $cm^2\ V^{-1}\ s^{-1}$), however was reduced compared to the non-fluorinated analogue ($\mu_{saturated}$ = 0.22 $cm^2\ V^{-1}\ s^{-1}$), which the authors were able to show was caused by increased surface roughness.[96] Nonetheless, the fluorinated polymer gave the best OPV efficiency when the two polymers were studied for their suitability as donor polymers. The improvement in open-circuit voltage and fill factor when using P15 allowed an optimum PCE of 4.4% to be achieved.[96] The contrasting performance trend when these polymers were used

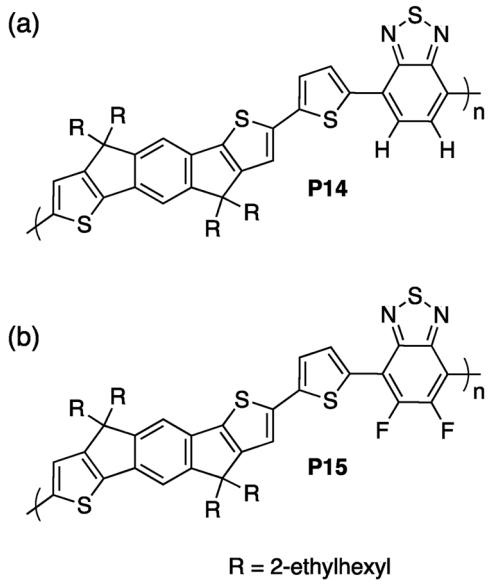

Figure 34. Structures of a) non-fluorinated and b) fluorinated polymers reported by Bronstein and co-workers to study the effect of fluorination on the benzothiadiazole-indacenodithiophene co-polymer.[96]

for OFETs and OPVs highlights that the use of non-covalent interactions in polymer design is not a one-stop solution for all optimization of organic semiconductor materials and properties such as solubility, bulk morphology and wettability, which are more difficult to predict, also have a strong influence on device performance.

Li and co-workers reported an interesting study in determining the effect of covalently or non-covalently locking the conformation of units in polymers by studying benzodithiophene-based polymers with ester functionalized thiophenes.[97] The co-polymers had different spacer groups in the polymer backbone, thieno[3,2-b]thiophene (P16) and 3,3'-difluoro-2,2'-thiophene (P17) (**Figure 35**a) to test the conformational locks.[97] The structures of model monomers determined by single crystal X-ray diffraction are shown in Figure 35b,c. The sulfur-fluorine interactions ensure that the bithiophene core is planar. However, the effect of the fluorine atoms extends to the intermolecular packing as it allows for stronger non-traditional hydrogen bonding between neighboring ester groups, reducing the dihedral angle between the core and the ester-functionalized thiophene group.[97] There is also the presence of H-F short contacts which can be expected to improve the interaction between polymer chains.[97]

Bulk heterojunction OPV devices, containing IT-4F as the acceptor, were fabricated for both polymers, with the sulfur-fluorine lock containing polymer, P17 achieving a PCE of 14.16%, significantly higher than the analogous polymer P16 (11.10%).[97] The parameters which are most improved are the short-circuit current density and the fill factor, demonstrating that the improved aggregation of P17 results in improved hole transport in the device.[97] In this case, the planarizing effect of sulfur-fluorine interactions assists with the optimized polymer chain packing, but this is in combination with non-traditional hydrogen bonding that is enhanced by the presence of fluorine atoms.

The effect of including heteroatoms in a polymer backbone isn't always as obvious as making the polymer chain more rigid or short heteroatom-heteroatom contact distances reducing the spacing between polymers chains. An example of this is reported by Jheng et al.[98] who detailed the study of a fluorinated polymer P19 (PTh_4FBT, **Figure 36**) which has a quaterthiophene-4, 5-difluoro-2, 1, 3-benzothiadiazole repeat unit. Compared to its non-fluorinated analogue, P18, where there are protons in the 5- and 6- positions of the benzothidiazole unit, P19 shows evidence of improved aggregation due to intermolecular interactions induced by the presence of the fluorine atoms.[98] Its melting point is 57 °C higher than P18, and its absorption profile has a more prominent shoulder at low energy, a signature of aggregation.[98] Additionally, unlike the spectrum of P18, this shoulder doesn't disappear with heating,[98] suggesting that the non-covalent intermolecular interactions in P19 are stronger. Further evidence for this was shown by powder X-ray diffraction where the spectrum for P19 displays peaks suggesting π-π stacking and an ordered long-range lamellar structure.[98] In contrast, P18 only shows an ordered lamellar structure after heating at 200 °C.[99] One of the main reasons attributed for improved aggregation is the enhanced dipole moment caused by the introduction of fluorine atoms as the magnitude and orientation of dipole moment has been credited for improved self-assembly.[45] In addition to this, however, it can be expected that the existence of sulfur-fluorine contacts, as detailed earlier, will also improve the aggregation in this polymer.

Despite there being examples showing the use of both intra- and intermolecular and sulfur-fluorine interactions in polymers, it is clear that these non-covalent contacts are not as influential in dictating conformation as sulfur-oxygen interactions. Kharandiuk et al. reported a series of EDOT-containing monomers which were designed with varying number of fluorine atoms in a central phenylene core to test the effect of sulfur-fluorine interactions.[100] These monomers were electropolymerized with the resulting polymers showing very different properties. Again, X-ray crystallography of the monomers was useful in relating the physical properties of the polymers to the presence or lack of intramolecular interactions, with the crystals structures presented in **Figure 37**a.

Monomer 1F shows disorder in the central phenylene group but the average torsion angle is determined to be 26.3°.[100] This is very slightly reduced compared to the analogous compound without any fluorine atoms on the phenylene core, reported by Sotzing and co-workers,[101] but the presence of one fluorine atom assists to create O···H–C contacts, due to its electron-withdrawing nature. Monomer 2F is planar with hydrogen bonds between the oxygens of the EDOT and the hydrogens of the core co-existing with the sulfur-fluorine interactions.[100] When a tetrafluorobenzene core is used in monomer 4F, the compound is highly twisted caused by repulsive oxygen-fluorine interactions, which are stronger than the attractive sulfur-fluorine interactions.[100] As a result, the resulting polymers poly(1F) and poly(2F) show absorbances strongly red-shifted compared to the monomers (Figure 37b), whereas poly(4F) does not show any absorbance above 350 nm, suggesting the highly twisted polymer caused disruption to conjugation in the polymer backbone.[100] The ionization energies of the polymers is influenced by a combination of the number of electronegative fluorine atoms and conjugation

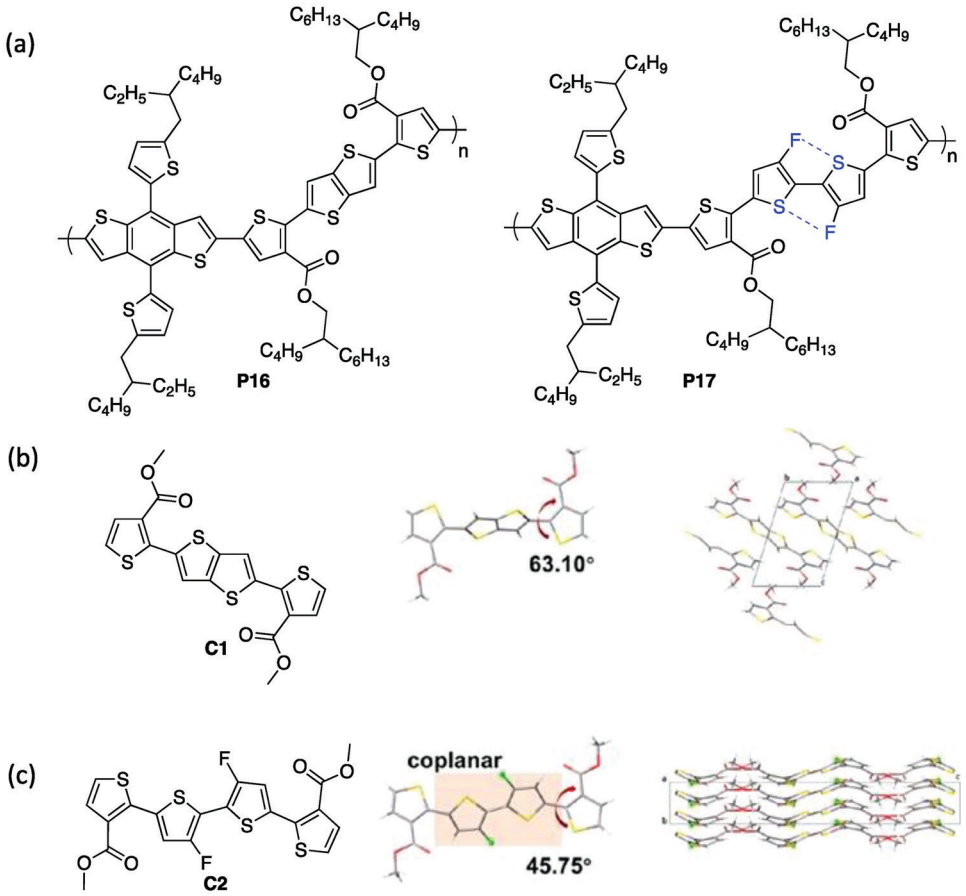

Figure 35. a) Structures of polymers P16 and P17; monomer control structures b) C1, with fused thieno[3,2-b]thiophene unit and c) C2, with sulfur-fluorine interactions. Reproduced with permission.[97] Copyright 2020, American Chemical Society.

length (Figure 37c).[100] The most planar polymer, poly(2F), had the lowest ionization energy (relative to vacuum) while the ionization energy of poly(4F) is significantly higher than the other polymers.[100]

Theoretical calculations carried out using the atoms-in-molecules approach showed that the sulfur-fluorine interactions are weak attractive and repulsive forces, where repulsion is caused from the steric effect of the fluorine atom.[100] This is consistent with a previous theoretical study by Thorley and McCulloch who concluded that S···F interactions are weaker than S···O interactions.[86] In these systems, the charge depleted area does not overlap well with the fluorine orbitals, therefore this should be considered when designing sulfur-fluorine interacting contacts. In this case, hydrogen bonding between the phenylene hydrogens and the oxygens of the EDOT unit are most influential in dictating the conformation.[100] It is common that there can be co-existing heteroatom-heteroatom interactions and hydrogen bonding in building blocks for semiconducting polymer materials, and the compatibility of these should be considered as part of the polymer design.

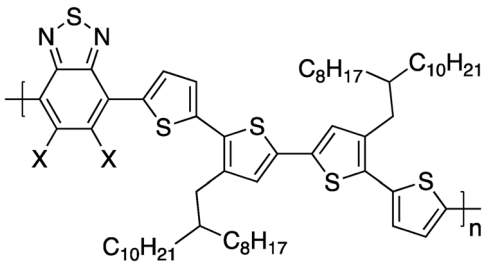

P18, X = H, **PTh$_4$BT**
P19, X= F, **PTh$_4$FBT**

Figure 36. Structure of fluorinated polymer P19 and its non-fluorinated analogue P18.

4.4. Hydrogen-Bonding in Polymers

While conventional hydrogen bonding, between hydrogen bond acceptor and donor groups (e.g., amides), has been used with great effect in improving the mechanical properties of organic semiconductor films such as flexibility and stretchability,[102] there has been a focus on designing polymers with unconventional hydrogen bonding for conformational control.

In 2013, Jackson and co-workers detailed how "non-traditional hydrogen bonding", between a heteroatom (acting as a hydrogen

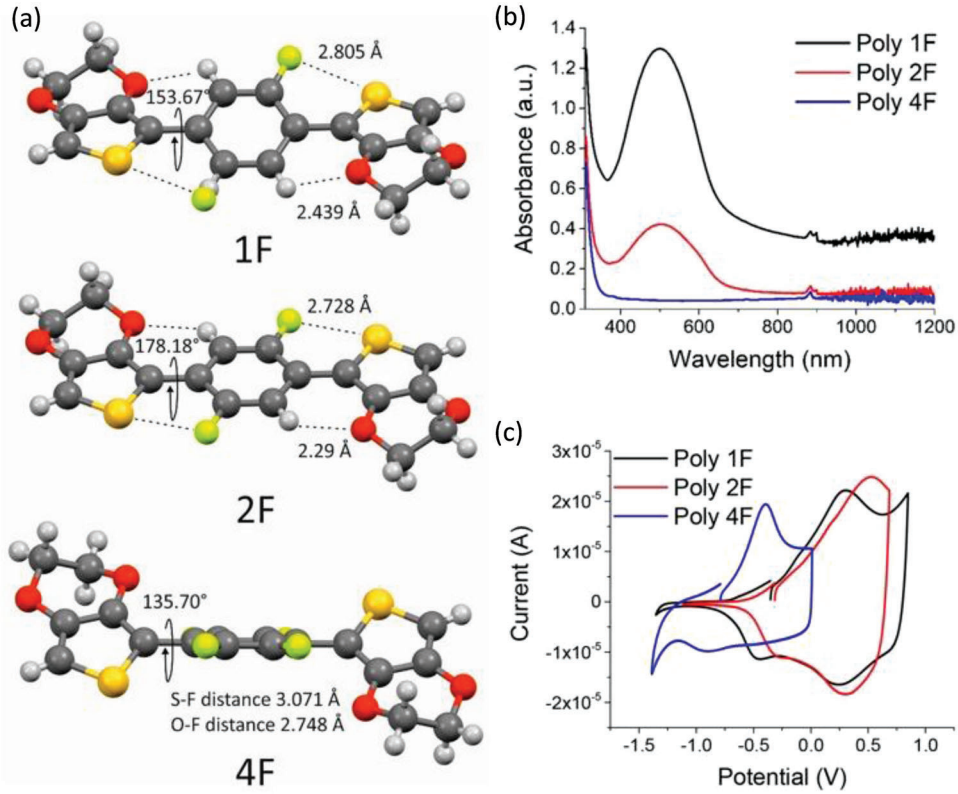

Figure 37. a) Structures of fluorine-containing monomers determined by single crystal X-ray diffraction; b) absorption spectra of resulting polymers synthesized by electropolymerization, and c) oxidation plots of electrodeposited polymers using cyclic voltammetry. Reproduced with permission.[100] Copyright 2019, American Chemical Society.

bond "acceptor") and hydrogen in a molecular/polymer backbone can exert conformational control of a planar structure preferentially over other non-covalent interactions.[103] This was an important observation as often non-traditional hydrogen bonding and other heteroatom interactions co-exist, and the non-traditional hydrogen bonding was often overlooked as a stabilizing interaction. Indeed, such interactions have been key to influencing the properties of many polymers. The work of Jackson et al., also highlighted that C–H···O and C–H···S interactions were typically influential, whereas C–H···F interactions, while capable of stabilizing interactions, are weaker.[103]

An example demonstrating the effectiveness of non-traditional hydrogen bonds was shown by Wang and co-workers who studied diketopyrrolopyrrole-based polymers (**Figure 38**a) to determine the influence of the hydrogen bonds.[104] A potential energy scan rotating around the dihedral angles between the thiophene/thiazole groups and the DPP core showed that the C–H···O interaction was most stable in the thiophene derivative, while a sulphur-oxygen interaction is most favourable in the thiazole analogue (Figure 38b).[104] When the polymers were used to fabricate n-type OFETs, P18 exhibited an electron mobility of 0.44 $cm^2\ V^{-1}\ s^{-1}$, which was ≈20 times higher than that determined for P19 (0.02 $cm^2\ V^{-1}\ s^{-1}$).[104] The authors used atomic force microscopy measurements to reveal the improved morphology, particularly after annealing at 300 °C for P18 and a combination of GIWAXS and solid-state NMR determined the improved crystallinity for P18 compared to P19, which was suggested to have a curved polymer backbone.[104]

Not only are these types of non-covalent interactions key to conformational control but there is also the possibility of improved inter-chain interactions. Typically, intramolecular interactions are used to flatten the polymer backbone and enhance intermolecular π-π stacking, while other intermolecular interactions such as hydrogen bonding can be used to influence the morphology of the bulk. A comparison effectiveness of inter- and intramolecular hydrogen bonding in polymers was nicely demonstrated by Ocheje and co-workers.[105] In this work, two DPP-thiophene-based polymers (**Figure 39**) were studied where the pyrazine and benzene units were placed in between two thiophene groups with amide side chains. This design enabled intramolecular hydrogen bonding in the pyrazine-containing polymer, P22, while only intermolecular hydrogen bonding could occur in the benzene-containing polymer, P23, due to an absence of H-bond acceptor atoms close to the amide side group.[105] The result is that P22 possesses a lower band gap and exhibited a higher hole mobility in organic field-effect transistors compared to P23.[105] The improved performance of P22 can be explained by improved rigidity, as shown by small angle neutron scattering (SANS) measurements of dilute solutions, and grazing-incidence wide-angle X-ray scattering (GIWAXS) measurements which showed improved crystallinity for polymer P22.[105] However, it was also determined from the GIWAXS study that the lamellar spacing was 25.1 and 23.3 Å for P22 and

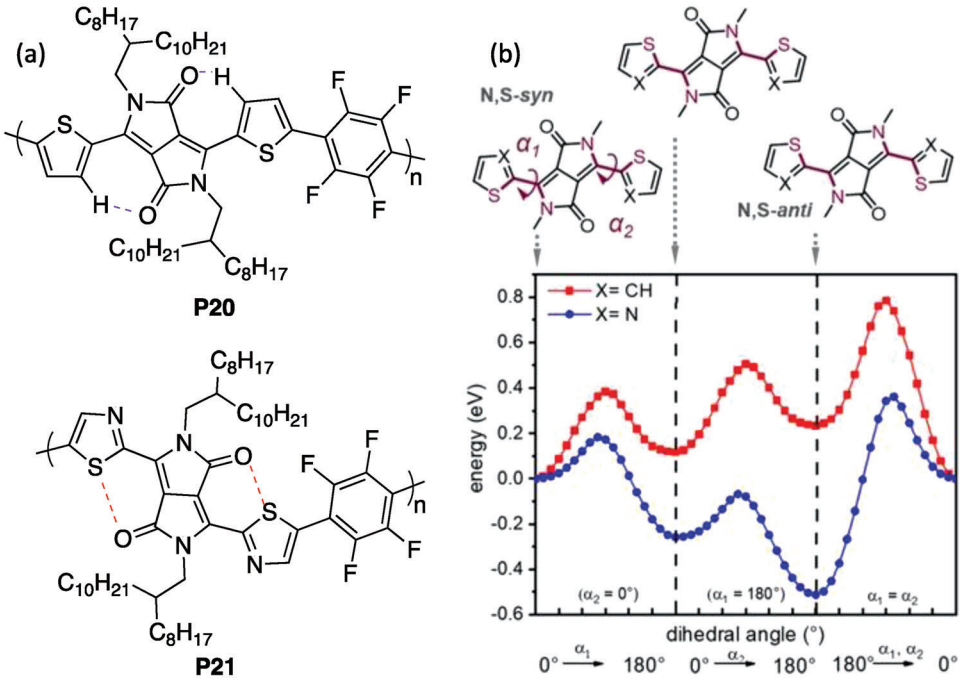

Figure 38. a) Structures of DPP-based polymers, P20 and P21, studied by Wang and co-workers to determine the influence non-traditional hydrogen bonding. Reproduced with permission.[104] Copyright 2021, American Chemical Society.

P23 respectively, highlighting that intramolecular hydrogen bonding is successful in bringing the polymer chains closer together.[105] The discrepancy in charge mobility for the two polymers emphasizes that rigidity of the polymer backbone, which promotes crystallinity, takes precedence over reducing the distance between the polymer chains in the pursuit of improved charge mobility.

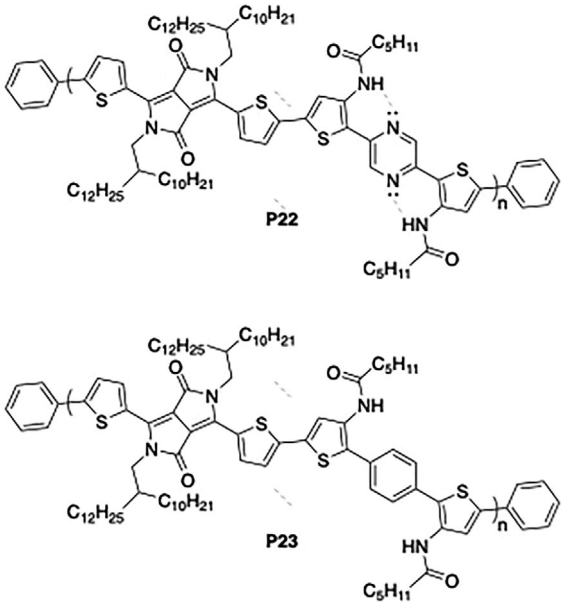

Figure 39. Structures of polymers P22 and P23 described by Ocheje et al. studying intra- and intermolecular hydrogen bonding.[105]

A strong class of intramolecular hydrogen bonding interactions used for conformational control of polymers is the resonance-assisted hydrogen bond (RAHB), where the interaction results in formation of a six membered ring and delocalization of the π-electrons. As a result, these types of interactions can be considered even stronger than conventional, electrostatic hydrogen bonds.[106] Therefore, RAHBs are a solid basis for conformational control in conjugated polymers. This was demonstrated effectively by Liu and co-workers, who showed that introducing an amide side chain in thiophene-thiazolothiazole-thiophene-based copolymers (**Figure 40**) can induce RAHBs which causes a 26× increase in the average hole mobility in OFETs.[107] The carbamate-containing polymer P25 has a band gap measurement in the thin film that is 0.15 eV lower in energy compared to P24.[107] Studies of the crystal structure of the RAHB-based monomer and previously reported thiophene-thiazolothiazole-thiophene structures showed that both types of monomer were planar, with sulfur-nitrogen and/or nitrogen-hydrogen interactions likely planarizing the dihedral angle between thiophene and thiazole units.[107] However, there is a vast difference in performance in p-type OFET devices, with P24-based OFETs giving an average hole mobility of 0.076 $cm^2\ V^{-1}\ s^{-1}$[108] and P25 containing transistors exhibiting an optimized, average hole mobility of 1.98 ($\pm$ 0.29) $cm^2\ V^{-1}\ s^{-1}$.[107] The improvement realized by inducing RAHBs is attributed to improved π electron delocalization but it is also likely that the stronger non-covalent interaction will cause fewer higher energy conformers to be present in the thin film, allowing for improved aggregation.

Competing non-traditional hydrogen bonding should be considered when polymers with heteroatom interactions are designed–in many cases the hydrogen bond will be energetically more stable than the heteroatom interaction, and therefore be

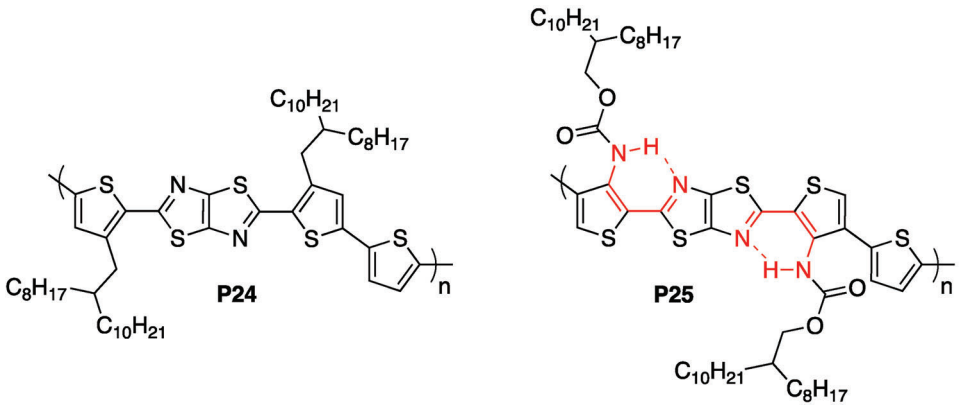

Figure 40. Structures of P24 and resonance-assisted hydrogen bond-containing analogue P25 reported by Liu and co-workers.[107]

more prevalent along the polymer backbone. However, these different classes of non-covalent interactions can work in synergy, as noted in how the electrostatic effect from fluorinated conformational locks can contribute to improved intermolecular non-traditional hydrogen bonding.[97] Therefore, although it is difficult to predict, synthetic chemists should look to enhance both kinds of interactions for effective intra- and interchain control of polymers.

However, chemists should not restrict themselves to hydrogen bonding which is inherently present in the polymer backbone. The advantage of organic semiconductor materials is the ease in which new structures can be created to attempt to improve device performance. The prevalence of semiconducting polymers containing five-membered ring heterocycles in their backbone is ripe for modification to introduce RAHBs, a strong interaction which has the potential to create stronger conformational control of polymers. As a result, polymers containing these interactions should be considered a promising class of future materials.

5. Summary

The variety of different interactions that have been shown to influence polymer conformation highlights that there is an array of design tools available for synthetic chemists to control the polymer structure to achieve desired physical properties for different semiconductor devices. These insights are hugely supported by single crystal X-ray diffraction studies of molecular-based organic semiconductors, where the different non-covalent interaction is often revealed in a single crystal structure. A subtle variation in molecular structure can dramatically change the crystal structure which defines the electronic properties of a small molecule organic semiconductor leading to different packing motifs with different dimensionalities of the stacking interactions. Sulfur-oxygen interactions are especially effective and new approaches to apply and manipulate these contacts can give rigidified structures but avoid the effect of increasing the ionization energy relative to vacuum. This allows such non-covalent interactions to be used in donor polymers for OPVs, where having a deep lying HOMO is desirable.

In the pursuit to study the influence of non-covalent interactions in polymers, full analysis of the monomer can go a long way to help predict the effect on the polymer material. However, as the examples above have shown, this should also be carried out in parallel with the design of analogous polymers with varying interactions to fully understand the effect of non-covalent interactions, particularly in the bulk. We have emphasized that the heteroatom interaction is absolutely responsible for bulk electronic properties, as shown by the examples of highly conducting BEDT-TTF salts, and highlighted research that shows that these interactions can be put to excellent use in the design of organic semiconductors with targeted properties.

Acknowledgements

The authors thank the EPSRC for funding under grants EP/R03480X/1 and EP/T022477/1.

Conflict of Interest

The authors declare no conflict of interest.

Keywords

heteroatom interactions, organic semiconductors, synthetic metals

Received: March 10, 2023
Revised: April 11, 2023
Published online:

[1] M. R. Bryce, *Chem. Soc. Rev.* **1991**, *20*, 355.
[2] P. J. Skabara, J.-B. Arlin, Y. H. Geerts, *Adv. Mater.* **2013**, *25*, 1948.
[3] J. R. Reynolds, A. J. Epstein, *Adv. Mater.* **2000**, *12*, 1565.
[4] H. Pang, F. Vilela, P. J. Skabara, J. J. W. McDouall, D. J. Crouch, T. D. Anthopoulos, D. D. C. Bradley, D. M. de Leeuw, P. N. Horton, M. B. Hursthouse, *Adv. Mater.* **2007**, *19*, 4438.
[5] C. Sutton, C. Risko, J.-L. Brédas, *Chem. Mater.* **2016**, *28*, 3.
[6] S. Scheiner, *Acc. Chem. Res.* **2013**, *46*, 280.
[7] R. Gleiter, G. Haberhauer, D. B. Werz, F. Rominger, C. Bleiholder, *Chem. Rev.* **2018**, *118*, 2010.
[8] L. C. Gilday, S. W. Robinson, T. A. Barendt, M. J. Langton, B. R. Mullaney, P. D. Beer, *Chem. Rev.* **2015**, *115*, 7118.
[9] T. J. Emge, M. A. Beno, C. A. Daws, H. H. Wang, J. M. Williams, *Mol. Cryst. Liq. Cryst.* **1984**, *116*, 153.

[10] M. Mantina, A. C. Chamberlin, R. Valero, C. J. Cramer, D. G. Truhlar, *J. Phys. Chem. A* **2009**, *113*, 5806.
[11] J. M. Williams, M. A. Beno, H. H. Wang, P. C. W. Leung, T. J. Emge, U. Geiser, K. D. Carlson, *Acc. Chem. Res.* **1985**, *18*, 261.
[12] J. M. Williams, M. A. Beno, J. C. Sullivan, L. M. Banovetz, J. M. Braam, G. S. Blackman, C. D. Carlson, D. L. Greer, D. M. Loesing, K. Carneiro, *Phys. Rev. B* **1983**, *28*, 2873.
[13] A. M. Kini, U. Geiser, H. H. Wang, K. D. Carlson, J. M. Williams, W. K. Kwok, K. G. Vandervoort, J. E. Thompson, D. L. Stupka, *Inorg. Chem.* **1990**, *29*, 2555.
[14] G. Conboy, H. J. Spencer, E. Angioni, A. L. Kanibolotsky, N. J. Findlay, S. J. Coles, C. Wilson, M. B. Pitak, C. Risko, V. Coropceanu, J.-L. Brédas, P. J. Skabara, *Mater. Horiz.* **2016**, *3*, 333.
[15] R. E. Martin, F. Diederich, *Angew. Chem., Int. Ed.* **1999**, *38*, 1350.
[16] H. Huang, L. Yang, A. Facchetti, T. J. Marks, *Chem. Rev.* **2017**, *117*, 10291.
[17] S. V. Meille, A. Farina, F. Bezziccheri, M. C. Gallazzi, *Adv. Mater.* **1994**, *6*, 848.
[18] N. Hergué, C. Mallet, G. Savitha, M. Allain, P. Frère, J. Roncali, *Org. Lett.* **2011**, *13*, 1762.
[19] J. Huang, Y. Tang, K. Gao, F. Liu, H. Guo, T. P. Russell, T. Yang, Y. Liang, X. Cheng, X. Guo, *Macromolecules* **2017**, *50*, 137.
[20] K. Yang, Q. Liao, J. Huang, Z. Zhang, M. Su, Z. Chen, Z. Wu, D. Wang, Z. Lai, H. Y. Woo, Y. Cao, P. Gao, X. Guo, *Angew. Chem., Int. Ed.* **2022**, *61*, 202113749.
[21] J.-M. Raimundo, P. Blanchard, P. Frère, N. Mercier, I. Ledoux-Rak, R. Hierle, J. Roncali, *Tetrahedron Lett.* **2001**, *42*, 1507.
[22] J. Roncali, P. Blanchard, P. Frère, *J. Mater. Chem.* **2005**, *15*, 1589.
[23] J.-M. Raimundo, P. Blanchard, N. Gallego-Planas, N. Mercier, I. Ledoux-Rak, R. Hierle, J. Roncali, *J. Org. Chem.* **2002**, *67*, 205.
[24] P. Leriche, M. Turbiez, V. Monroche, P. Frère, P. Blanchard, P. J. Skabara, J. Roncali, *Tetrahedron Lett.* **2003**, *44*, 649.
[25] C. B. Nielsen, A. Angerhofer, K. A. Abboud, J. R. Reynolds, *J. Am. Chem. Soc.* **2008**, *130*, 9734.
[26] T. Matsuo, K. Kawabata, K. Takimiya, *Bull. Chem. Soc. Jpn.* **2022**, *95*, 1047.
[27] H. Zhang, W. Xu, K. Song, T. Lu, G. Zhang, Y. Zang, W. Hong, D. Zhang, *Adv. Sci.* **2022**, *9*, 2105667.
[28] H. Huang, Z. Chen, R. P. Ortiz, C. Newman, H. Usta, S. Lou, J. Youn, Y.-Y. Noh, K.-J. Baeg, L. X. Chen, A. Facchetti, T. Marks, *J. Am. Chem. Soc.* **2012**, *134*, 10966.
[29] L. Yang, P. Ye, W. Li, W. Zhang, Q. Guan, C. Ye, T. Dong, X. Wu, W. Zhao, X. Gu, Q. Peng, B. Tang, H. Huang, *Adv. Optical Mater.* **2018**, *6*, 1701394.
[30] a) J. Duan, G. Zhu, L. Wang, J. Chen, S. Cong, X. Zhu, Y. Zhou, Z. Li, I. McCulloch, W. Yue, *Adv. Funct. Mater.* **2022**, *32*, 2203937; b) G. Zhu, J. Chen, J. Duan, H. Liao, X. Zhu, Z. Li, I. McCulloch, W. Yue, *ACS Appl. Mater. Interfaces* **2022**, *14*, 43586; c) J. Duan, G. Zhu, L. Lan, J. Chen, X. Zhu, C. Chen, Y. Yu, H. Liao, Z. Li, I. McCulloch, W. Yue, *Angew. Chem., Int. Ed.* **2023**, *62*, 202213737.
[31] G.-Y. Ge, J.-T. Li, J.-R. Wang, M. Xiong, X. Dong, Z.-J. Li, J.-L. Li, X.-Y. Cao, T. Lei, J.-L. Wang, *Adv. Funct. Mater.* **2022**, *32*, 2108289.
[32] a) N. J. Hestand, F. C. Spano, *Chem. Rev.* **2018**, *118*, 7069; b) A. L. Kanibolotsky, F. Vilela, J. C. Forgie, S. E. T. Elmasly, P. J. Skabara, K. Zhang, B. Tieke, J. McGurk, C. R. Belton, P. N. Stavrinou, D. D. C. Bradley, *Adv. Mater.* **2011**, *23*, 2093.
[33] Y. Patil, R. Misra, *J. Mater. Chem. C* **2019**, *7*, 13020.
[34] W. S. Yoon, D. W. Kim, J.-M. Park, I. Cho, O. K. Kwon, D. R. Whang, J. H. Kim, J.-H. Park, S. Y. Park, *Macromolecules* **2016**, *49*, 8489.
[35] M.-W. Choi, G. Kim, A. Seitkazina, S.-Y. Kim, W. S. Yoon, J. E. Kwon, S. Kim, S. Y. Park, *Dyes Pigm.* **2022**, *207*, 110699.
[36] Y. Lin, J. Wang, Z.-G. Zhang, H. Bai, Y. Li, D. Zhu, X. Zhan, *Adv. Mater.* **2015**, *27*, 1170.
[37] J. Yuan, Y. Zhang, L. Zhou, G. Zhang, H.-L. Yip, T.-K. Lau, X. Lu, C. Zhu, H. Peng, P. A. Johnson, M. Leclerc, Y. Cao, J. Ulanski, Y. Li, Y. Zou, *Joule* **2019**, *3*, 1140.
[38] L. Ma, S. Zhang, J. Hou, *J. Mater. Chem. A* **2023**, *11*, 481.
[39] J. Zhou, D. He, Y. Li, F. Huang, J. Zhang, C. Zhang, Y. Yuan, Y. Lin, C. Wang, F. Zhao, *Adv. Mater.* **2023**, *35*, 2207336.
[40] Y. Shi, Y. Chang, K. Lu, Z. Chen, J. Zhang, Y. Yan, D. Qiu, Y. Liu, M. A. Adil, W. Ma, X. Hao, L. Zhu, Z. Wei, *Nat. Commun.* **2022**, *13*, 3256.
[41] S. Feng, M. Li, N. Tang, X. Wang, H. Huang, G. Ran, Y. Liu, Z. Xie, W. Zhang, Z. Bo, *ACS Appl. Mater. Interfaces* **2020**, *12*, 4638.
[42] R. G. D. Taylor, J. Cameron, I. A. Wright, N. Thomson, O. Avramchenko, A. L. Kanibolotsky, A. R. Inigo, T. Tuttle, P. J. Skabara, *Beilstein J. Org. Chem.* **2015**, *11*, 1148.
[43] I. A. Wright, N. J. Findlay, S. Arumugam, A. R. Inigo, A. L. Kanibolotsky, P. Zassowski, W. Domagala, P. J. Skabara, *J. Mater. Chem. C* **2014**, *2*, 2674.
[44] M. Mamada, H. Fujita, K. Kakita, H. Shima, Y. Yoneda, Y. Tanaka, S. Tokito, *New J. Chem.* **2016**, *40*, 1403.
[45] C. J. Takacs, Y. Sun, G. C. Welch, L. A. Perez, X. Liu, W. Wen, G. C. Bazan, A. J. Heeger, *J. Am. Chem. Soc.* **2012**, *134*, 16597.
[46] A. Zhugayevych, O. Postupna, R. C. Bakus Ii, G. C. Welch, G. C. Bazan, S. Tretiak, *J. Phys. Chem. C* **2013**, *117*, 4920.
[47] G. C. Welch, R. C. Bakus, II, S. J. Teat, G. C. Bazan, *J. Am. Chem. Soc.* **2013**, *135*, 2298.
[48] J. Jiang, Z. Xu, J. Zhou, M. Hanif, Q. Jiang, D. Hu, R. Zhao, C. Wang, L. Liu, D. Ma, Y. Ma, Y. Cao, *Chem. Mater.* **2019**, *31*, 6499.
[49] a) M. Kasha, H. R. Rawls, M. A. El-Bayoumi, *Pure Appl. Chem.* **1965**, *11*, 371; b) V. H. K. Fell, J. Cameron, A. L. Kanibolotsky, E. J. Hussien, P. J. Skabara, *Beilstein J. Org. Chem.* **2022**, *18*, 944; c) H. Yang, J. Bruckbauer, L. Kanibolotska, A. L. Kanibolotsky, J. Cameron, D. J. Wallis, R. W. Martin, P. J. Skabara, *J. Mater. Chem. C* **2023**, https://doi.org/10.1039/d2tc05139g.
[50] V. M. Korshunov, T. N. Chmovzh, A. Y. Freidzon, M. E. Minyaev, A. D. Barkanov, I. S. Golovanov, L. V. Mikhalchenko, I. C. Avetisov, I. V. Taydakov, O. A. Rakitin, *Dyes Pigm.* **2022**, *208*, 110860.
[51] Y. Sakamoto, S. Komatsu, T. Suzuki, *J. Am. Chem. Soc.* **2001**, *123*, 4643.
[52] L.-H. Wang, X.-J. Chen, D.-N. Ye, H. Liu, Y. Chen, A.-G. Zhong, C.-Z. Li, S.-Y. Liu, *Polym. Chem.* **2022**, *13*, 2351.
[53] Z. Wang, M. Huang, J. Dong, X. Wang, Y. Li, M. Sun, S. Chang, *J. Phys. Chem. C* **2023**, *127*, 2518.
[54] Y. Wang, S. R. Parkin, J. Gierschner, M. D. Watson, *Org. Lett.* **2008**, *10*, 3307.
[55] D. Romito, E. Fresta, L. M. Cavinato, H. Kählig, H. Amenitsch, L. Caputo, Y. Chen, P. Samorì, J.-C. Charlier, R. D. Costa, D. Bonifazi, *Angew. Chem., Int. Ed.* **2022**, *61*, 202202137.
[56] M. Irimia-Vladu, E. D. Głowacki, P. A. Troshin, G. Schwabegger, L. Leonat, D. K. Susarova, O. Krystal, M. Ullah, Y. Kanbur, M. A. Bodea, V. F. Razumov, H. Sitter, S. Bauer, N. S. Sariciftci, *Adv. Mater.* **2012**, *24*, 375.
[57] a) E. D. Głowacki, L. Leonat, G. Voss, M.-A. Bodea, Z. Bozkurt, A. M. Ramil, M. Irimia-Vladu, S. Bauer, N. S. Sariciftci, *AIP Adv.* **2011**, *1*, 042132; b) Y. Kanbur, M. Irimia-Vladu, E. D. Głowacki, G. Voss, M. Baumgartner, G. Schwabegger, L. Leonat, M. Ullah, H. Sarica, S. Erten-Ela, R. Schwödiauer, H. Sitter, Z. Küçükyavuz, S. Bauer, N. S. Sariciftci, *Org. Electron.* **2012**, *13*, 919.
[58] F. Kettner, L. Huter, J. Schafer, K. Roder, U. Purgahn, H. Krautscheid, *Acta Crystallogr F Struct Biol Commun* **2011**, *67*, o2867.
[59] S. Larsen, F. Wätjen, *Acta Chem. Scand.* **1980**, *34a*, 171.
[60] O. Pitayatanakul, T. Higashino, T. Kadoya, M. Tanaka, H. Kojima, M. Ashizawa, T. Kawamoto, H. Matsumoto, K. Ishikawa, T. Mori, *J. Mater. Chem. C* **2014**, *2*, 9311.
[61] G. Cavallo, P. Metrangolo, R. Milani, T. Pilati, A. Priimagi, G. Resnati, G. Terraneo, *Chem. Rev.* **2016**, *116*, 2478.

[62] O. P. Lee, A. T. Yiu, P. M. Beaujuge, C. H. Woo, T. W. Holcombe, J. E. Millstone, J. D. Douglas, M. S. Chen, J. M. J. Fréchet, *Adv. Mater.* **2011**, *23*, 5359.
[63] a) J. Liu, B. Walker, A. Tamayo, Y. Zhang, T.-Q. Nguyen, *Adv. Funct. Mater.* **2013**, *23*, 47; b) J. Liu, Y. Zhang, H. Phan, A. Sharenko, P. Moonsin, B. Walker, V. Promarak, T.-Q. Nguyen, *Adv. Mater.* **2013**, *25*, 3645.
[64] J.-H. Dou, Y.-Q. Zheng, Z.-F. Yao, T. Lei, X. Shen, X.-Y. Luo, Z.-A. Yu, S.-D. Zhang, G. Han, Z. Wang, Y. Yi, J.-Y. Wang, J. Pei, *Adv. Mater.* **2015**, *27*, 8051.
[65] Z.-P. Yu, Z.-X. Liu, F.-X. Chen, R. Qin, T.-K. Lau, J.-L. Yin, X. Kong, X. Lu, M. Shi, C.-Z. Li, H. Chen, *Nat. Commun.* **2019**, *10*, 2152.
[66] T.-J. Wen, Z.-X. Liu, Z. Chen, J. Zhou, Z. Shen, Y. Xiao, X. Lu, Z. Xie, H. Zhu, C.-Z. Li, H. Chen, *Angew. Chem., Int. Ed.* **2021**, *60*, 12964.
[67] Z.-X. Liu, Z.-P. Yu, Z. Shen, C. He, T.-K. Lau, Z. Chen, H. Zhu, X. Lu, Z. Xie, H. Chen, C.-Z. Li, *Nat. Commun.* **2021**, *12*, 3049.
[68] a) S. Holliday, R. S. Ashraf, A. Wadsworth, D. Baran, S. A. Yousaf, C. B. Nielsen, C.-H. Tan, S. D. Dimitrov, Z. Shang, N. Gasparini, M. Alamoudi, F. Laquai, C. J. Brabec, A. Salleo, J. R. Durrant, I. McCulloch, *Nat. Commun.* **2016**, *7*, 11585; b) S. Strohm, F. Machui, S. Langner, P. Kubis, N. Gasparini, M. Salvador, I. McCulloch, H. J. Egelhaaf, C. J. Brabec, *Energy Environ. Sci.* **2018**, *11*, 2225; c) M. T. Dang, L. Hirsch, G. Wantz, *Adv. Mater.* **2011**, *23*, 3597.
[69] a) Z. Bao, A. Dodabalapur, A. J. Lovinger, *Appl. Phys. Lett.* **1996**, *69*, 4108; b) R. J. Kline, M. D. McGehee, E. N. Kadnikova, J. Liu, J. M. J. Fréchet, *Adv. Mater.* **2003**, *15*, 1519; c) L. Janasz, D. Chlebosz, M. Gradzka, W. Zajaczkowski, T. Marszalek, K. Müllen, J. Ulanski, A. Kiersnowski, W. Pisula, *J. Mater. Chem. C* **2016**, *4*, 11488.
[70] a) S. Mun, Y. Park, Y.-E. K. Lee, M. M. Sung, *Langmuir* **2017**, *33*, 13554; b) S. Han, X. Zhuang, W. Shi, X. Yang, L. Li, J. Yu, *Sens. Actuators, B* **2016**, *225*, 10.
[71] T.-A. Chen, X. Wu, R. D. Rieke, *J. Am. Chem. Soc.* **1995**, *117*, 233.
[72] R. D. McCullough, R. D. Lowe, *J. Chem. Soc., Chem. Commun.* **1992**, 70.
[73] T. A. Chen, R. D. Rieke, *J. Am. Chem. Soc.* **1992**, *114*, 10087.
[74] T. M. McCormick, C. R. Bridges, E. I. Carrera, P. M. DiCarmine, G. L. Gibson, J. Hollinger, L. M. Kozycz, D. S. Seferos, *Macromolecules* **2013**, *46*, 3879.
[75] G. H. F. Jonas, W. Schmidtberg, J. Heinze, M. Dietrich, Vol. EP0203438A1 (Ed.: E. P. Office), Bayer AG, **1989**.
[76] G. Heywang, F. Jonas, *Adv. Mater.* **1992**, *4*, 116.
[77] M. Turbiez, P. Frère, P. Blanchard, J. Roncali, *Tetrahedron Lett.* **2000**, *41*, 5521.
[78] G. J. McEntee, P. J. Skabara, F. Vilela, S. Tierney, I. D. W. Samuel, S. Gambino, S. J. Coles, M. B. Hursthouse, R. W. Harrington, W. Clegg, *Chem. Mater.* **2010**, *22*, 3000.
[79] X. Guo, Q. Liao, E. F. Manley, Z. Wu, Y. Wang, W. Wang, T. Yang, Y.-E. Shin, X. Cheng, Y. Liang, L. X. Chen, K.-J. Baeg, T. J. Marks, X. Guo, *Chem. Mater.* **2016**, *28*, 2449.
[80] A. Giovannitti, D.-T. Sbircea, S. Inal, C. B. Nielsen, E. Bandiello, D. A. Hanifi, M. Sessolo, G. G. Malliaras, I. McCulloch, J. Rivnay, *Proc. Natl. Acad. Sci. USA* **2016**, *113*, 12017.
[81] P. R. Paudel, J. Tropp, V. Kaphle, J. D. Azoulay, B. Lüssem, *J. Mater. Chem. C* **2021**, *9*, 9761.
[82] M. C. Scharber, D. Mühlbacher, M. Koppe, P. Denk, C. Waldauf, A. J. Heeger, C. J. Brabec, *Adv. Mater.* **2006**, *18*, 789.
[83] G. S. Sinclair, R. C. M. Claridge, A. J. Kukor, W. S. Hopkins, D. J. Schipper, *Chem. Sci.* **2021**, *12*, 2304.
[84] J. Chen, Q. Liao, G. Wang, Z. Yan, H. Wang, Y. Wang, X. Zhang, Y. Tang, A. Facchetti, T. J. Marks, X. Guo, *Macromolecules* **2018**, *51*, 3874.
[85] X. Guo, N. Zhou, S. J. Lou, J. W. Hennek, R. Ponce Ortiz, M. R. Butler, P.-L. T. Boudreault, J. Strzalka, P.-O. Morin, M. Leclerc, J. T. López Navarrete, M. A. Ratner, L. X. Chen, R. P. H. Chang, A. Facchetti, T. J. Marks, *J. Am. Chem. Soc.* **2012**, *134*, 18427.
[86] K. J. Thorley, I. McCulloch, *J. Mater. Chem. C* **2018**, *6*, 12413.
[87] H. Bronstein, M. Hurhangee, E. C. Fregoso, D. Beatrup, Y. W. Soon, Z. Huang, A. Hadipour, P. S. Tuladhar, S. Rossbauer, E.-H. Sohn, S. Shoaee, S. D. Dimitrov, J. M. Frost, R. S. Ashraf, T. Kirchartz, S. E. Watkins, K. Song, T. Anthopoulos, J. Nelson, B. P. Rand, J. R. Durrant, I. McCulloch, *Chem. Mater.* **2013**, *25*, 4239.
[88] B. Fu, C.-Y. Wang, B. D. Rose, Y. Jiang, M. Chang, P.-H. Chu, Z. Yuan, C. Fuentes-Hernandez, B. Kippelen, J.-L. Brédas, D. M. Collard, E. Reichmanis, *Chem. Mater.* **2015**, *27*, 2928.
[89] C. Buckley, S. Thomas, M. McBride, Z. Yuan, G. Zhang, J.-L. Bredas, E. Reichmanis, *Chem. Mater.* **2019**, *31*, 3957.
[90] B. Liu, D. Rocca, H. Yan, D. Pan, *JACS Au* **2021**, *1*, 2182.
[91] Z. He, B. Xiao, F. Liu, H. Wu, Y. Yang, S. Xiao, C. Wang, T. P. Russell, Y. Cao, *Nat. Photonics* **2015**, *9*, 174.
[92] Y. Liu, J. Zhao, Z. Li, C. Mu, W. Ma, H. Hu, K. Jiang, H. Lin, H. Ade, H. Yan, *Nat. Commun.* **2014**, *5*, 5293.
[93] M. Zhang, X. Guo, W. Ma, H. Ade, J. Hou, *Adv. Mater.* **2015**, *27*, 4655.
[94] J. Wang, Z. Zheng, Y. Zu, Y. Wang, X. Liu, S. Zhang, M. Zhang, J. Hou, *Adv. Mater.* **2021**, *33*, 2102787.
[95] a) Y. Zhang, S.-C. Chien, K.-S. Chen, H.-L. Yip, Y. Sun, J. A. Davies, F.-C. Chen, A. K. Y. Jen, *Chem. Commun.* **2011**, *47*, 11026; b) G. K. Dutta, T. Kim, H. Choi, J. Lee, D. S. Kim, J. Y. Kim, C. Yang, *Polym. Chem.* **2014**, *5*, 1243.
[96] H. Bronstein, J. M. Frost, A. Hadipour, Y. Kim, C. B. Nielsen, R. S. Ashraf, B. P. Rand, S. Watkins, I. McCulloch, *Chem. Mater.* **2013**, *25*, 277.
[97] S. Li, W. Zhao, J. Zhang, X. Liu, Z. Zheng, C. He, B. Xu, Z. Wei, J. Hou, *Chem. Mater.* **2020**, *32*, 1993.
[98] J.-F. Jheng, Y.-Y. Lai, J.-S. Wu, Y.-H. Chao, C.-L. Wang, C.-S. Hsu, *Adv. Mater.* **2013**, *25*, 2445.
[99] K.-H. Ong, S.-L. Lim, J. Li, H.-K. Wong, H.-S. Tan, T.-T. Lin, L. C. H. Moh, J. C. de Mello, Z.-K. Chen, *Polym. Chem.* **2013**, *4*, 1863.
[100] T. Kharandiuk, E. J. Hussien, J. Cameron, R. Petrina, N. J. Findlay, R. Naumov, W. T. Klooster, S. J. Coles, Q. Ai, S. Goodlett, C. Risko, P. J. Skabara, *Chem. Mater.* **2019**, *31*, 7070.
[101] G. A. Sotzing, J. R. Reynolds, P. J. Steel, *Chem. Mater.* **1996**, *8*, 882.
[102] L. Bai, Y. Han, C. Sun, X. An, C. Wei, W. Liu, M. Xu, L. Sun, N. Sun, M. Yu, H. Zhang, Q. Wei, C. Xu, Y. Yang, T. Qin, L. Xie, J. Lin, W. Huang, *Research* **2020**, *2020*, 3405826.
[103] N. E. Jackson, B. M. Savoie, K. L. Kohlstedt, M. Olvera de la Cruz, G. C. Schatz, L. X. Chen, M. A. Ratner, *J. Am. Chem. Soc.* **2013**, *135*, 10475.
[104] Q. Wang, S. Böckmann, F. Günther, M. Streiter, M. Zerson, A. D. Scaccabarozzi, W. L. Tan, H. Komber, C. Deibel, R. Magerle, S. Gemming, C. R. McNeill, M. Caironi, M. R. Hansen, M. Sommer, *Chem. Mater.* **2021**, *33*, 2635.
[105] M. U. Ocheje, R. B. Goodman, K.-T. Lu, Y. Wang, L. A. Galuska, L. Soullard, Z. Cao, S. Zhang, M. Yadiki, X. Gu, Y.-C. Chiu, S. Rondeau-Gagné, *Chem. Mater.* **2021**, *33*, 8267.
[106] P. Gilli, V. Bertolasi, V. Ferretti, G. Gilli, *J. Am. Chem. Soc.* **1994**, *116*, 909.
[107] B. Liu, J. Li, W. Zeng, W. Yang, H. Yan, D.-c. Li, Y. Zhou, X. Gao, Q. Zhang, *Chem. Mater.* **2021**, *33*, 580.
[108] I. Osaka, R. Zhang, J. Liu, D.-M. Smilgies, T. Kowalewski, R. D. McCullough, *Chem. Mater.* **2010**, *22*, 4191.

Joseph Cameron was awarded his PhD in 2016 from the University of Strathclyde under the supervision of Professor Peter Skabara. He worked as a postdoctoral researcher at the University of Strathclyde until 2018 when he moved to the University of Glasgow as a research associate in the group of Prof. Skabara, where he is currently working. His research interests include organic synthesis of functional materials and the development of organic semiconductor devices.

Alexander Kanibolotsky obtained his PhD from the Institute of Physical Organic Chemistry and Coal Chemistry of the National Academy of Science in Ukraine (NASU). He worked as a postdoctoral researcher in the group of Professor Skabara at the University of Manchester and Professor Alan Gorgues at the University of Angers, France. Currently on leave from NASU, he is a senior researcher in the group of Professor Skabara at the University of Glasgow.

Peter Skabara completed his PhD studies in 1994 under the supervision of Professor Martin Bryce at the University of Durham before taking up a Max-Planck Fellowship with Professor Klaus Müllen at the MPI for Polymer Research in Mainz (1994-95). His academic career began at Sheffield Hallam University in 1995, and he moved to the University of Manchester, before joining the University of Strathclyde (2005-18). In 2018 he moved from Strathclyde to his present position as the Ramsay Chair of Chemistry at the University of Glasgow.